

AD-A061 470

PENNSYLVANIA STATE UNIV UNIVERSITY PARK APPLIED RESE--ETC F/G 20/4
EXPERIMENTAL AXISYMMETRIC BOUNDARY-LAYER PROFILE MODIFICATIONS --ETC(U)
MAR 78 B E ROBBINS

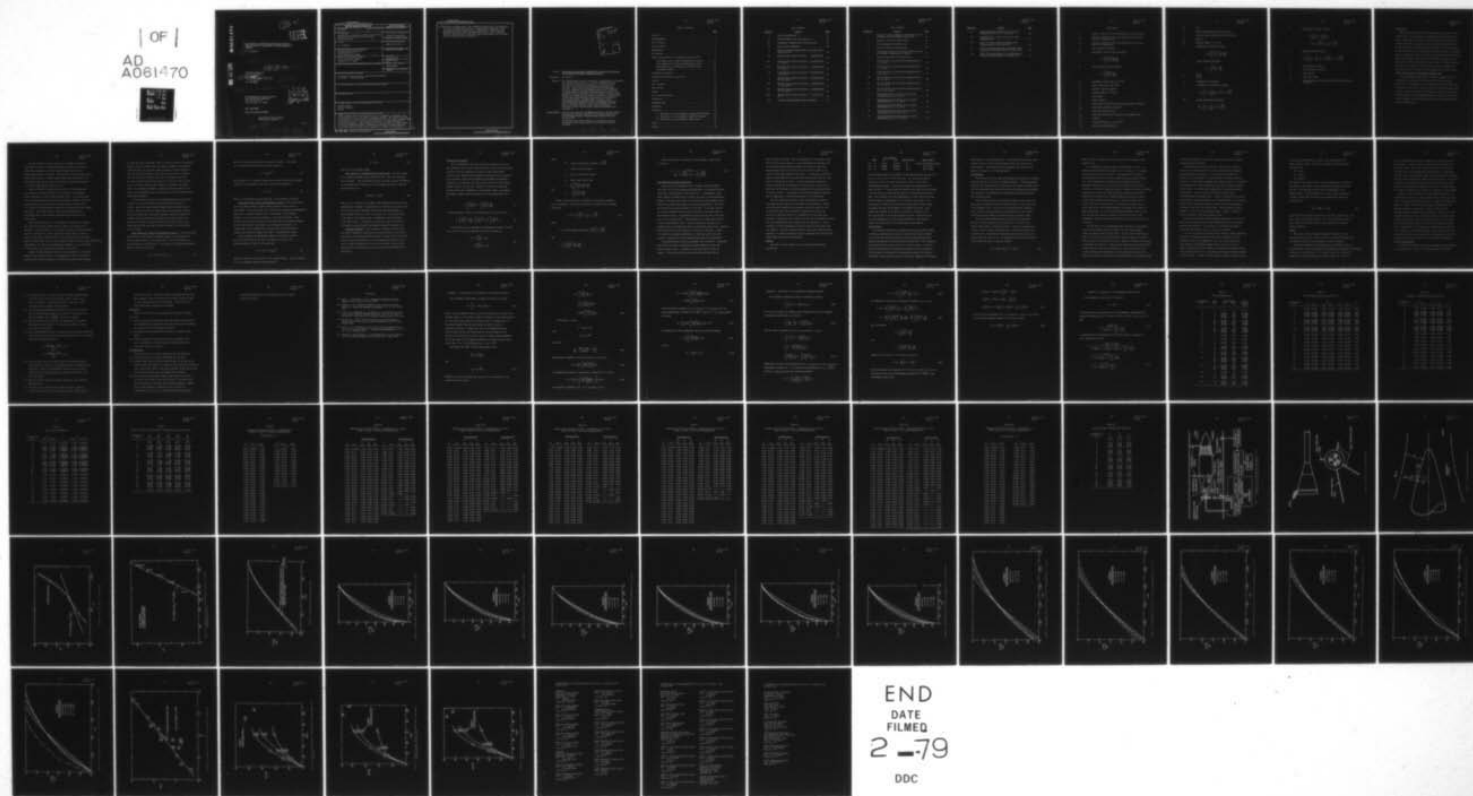
UNCLASSIFIED

ARL/PSU-TM-78-64

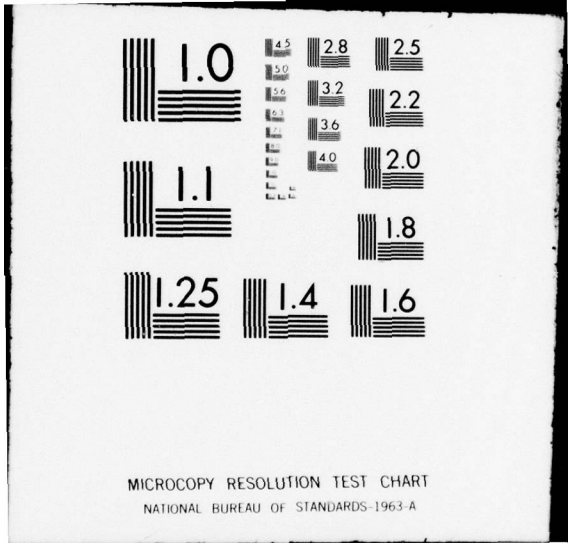
N00017-73-C-1418

NL

| OF |
AD
A061470



END
DATE
FILMED
2 -79
DDC



ADA061470

DDC FILE COPY

12 ←

LEVEL

6

EXPERIMENTAL AXISYMMETRIC BOUNDARY-LAYER PROFILE
MODIFICATIONS BY THE ADDITION OF SURFACE ROUGHNESS
SCREENS.

10 B. E./Robbins

9 Technical memo.

14 ARL PSU-TM-78-64

Technical Memorandum
File No. TM 78-64
24 March 1978
Contract No. N00017-73-C-1418
Copy No. 40

11

15

12 76p.

16 F43421

17 ZF43421041

The Pennsylvania State University
APPLIED RESEARCH LABORATORY
Post Office Box 30
State College, PA 16801

DDC
RECEIVED
NOV 24 1978
A

NAVY DEPARTMENT
NAVAL SEA SYSTEMS COMMAND

Approved for Public Release
Distribution Unlimited

391 007

JOB

8 11 20 090

UNCLASSIFIED

SECURITY CLASSIFICATION OF THIS PAGE (When Data Entered)

REPORT DOCUMENTATION PAGE		READ INSTRUCTIONS BEFORE COMPLETING FORM
1. REPORT NUMBER TM 78-64	2. GOVT ACCESSION NO.	3. RECIPIENT'S CATALOG NUMBER
4. TITLE (and Subtitle) Experimental Axisymmetric Boundary-Layer Profile Modifications by the Addition of Surface Roughness Screens		5. TYPE OF REPORT & PERIOD COVERED Technical Memorandum
		6. PERFORMING ORG. REPORT NUMBER
7. AUTHOR(s) B. E. Robbins		8. CONTRACT OR GRANT NUMBER(s) N00017-73-C-1418
9. PERFORMING ORGANIZATION NAME AND ADDRESS Applied Research Laboratory Post Office Box 30 State College, PA 16801		10. PROGRAM ELEMENT, PROJECT, TASK AREA & WORK UNIT NUMBERS
11. CONTROLLING OFFICE NAME AND ADDRESS Naval Sea Systems Command Washington, DC 20362		12. REPORT DATE 24 March 1978
		13. NUMBER OF PAGES 70
14. MONITORING AGENCY NAME & ADDRESS (if different from Controlling Office)		15. SECURITY CLASS. (of this report) UNCLASSIFIED
		15a. DECLASSIFICATION/DOWNGRADING SCHEDULE
16. DISTRIBUTION STATEMENT (of this Report) Approved for Public Release - Distribution Unlimited Per NAVSEA - 26 October 1978		
17. DISTRIBUTION STATEMENT (of the abstract entered in Block 20, if different from Report)		
18. SUPPLEMENTARY NOTES		
19. KEY WORDS (Continue on reverse side if necessary and identify by block number) boundary layer surface roughness screen		
20. ABSTRACT (Continue on reverse side if necessary and identify by block number) The boundary-layer velocity profile on an axisymmetric aerodynamic body was modified by the use of surface roughness screens. The velocity profiles were measured at a body location of $x/L=0.970$ for various screen configurations placed near the nose. These results obtained in air, were determined to allow the simulation of the boundary-layer velocity profile on longer models at different Reynolds numbers. Results were obtained for three different screen mesh sizes and three screen lengths up to 60.96 cm (24 inches) in		

DD FORM 1 JAN 73 1473

EDITION OF 1 NOV 65 IS OBSOLETE

UNCLASSIFIED

SECURITY CLASSIFICATION OF THIS PAGE (When Data Entered)

UNCLASSIFIED

SECURITY CLASSIFICATION OF THIS PAGE(When Data Entered)

20. ↘ different configurations. The following boundary-layer characteristics are given for each configuration: boundary-layer thickness, planar displacement and momentum thickness, axisymmetric displacement and momentum thickness, planar and axisymmetric shape factor, friction velocity, skin friction coefficient, wall shear stress, and the planar universal boundary-layer parameters. ↗

UNCLASSIFIED

SECURITY CLASSIFICATION OF THIS PAGE(When Data Entered)

Table of Contents

	<u>Page</u>
Abstract	1
Acknowledgments	1
List of Tables	3
List of Figures	4
Nomenclature	6
Introduction	9
General Characteristics of Turbulent Boundary Layers	9
Inner Region Over a Smooth Two-Dimensional Surface	11
Inner Region Over a Rough Two-Dimensional Surface	12
Outer Region of a Two-Dimensional Boundary Layer	13
Axisymmetric Bodies	13
Parameters for Analysis	14
Instrumentation and Data Acquisition	16
Screens	17
Test Procedure	18
Data Analysis	19
Results	22
Use of the Screen Data	23
Conclusions	25
Recommendations	25
References	27
Appendices	28
A. Derivation of the Axisymmetric Displacement Thickness	28
B. Derivation of the Axisymmetric Momentum Thickness	31
C. Derivation of the Axisymmetric Shape Factor	34
Tables	35
Figures	49

List of Tables

<u>Table No.</u>	<u>Caption</u>	<u>Page</u>
I	Screen Configurations	35
II	Planar Boundary-Layer Characteristics	36
III	Axisymmetric Boundary-Layer Characteristics	37
IV	Skin Friction Parameters	38
V	Effect of Screen Configurations on Boundary-Layer Characteristics	39
VI	Boundary-Layer Velocity Profile -- Configuration 0	40
VII	Boundary-Layer Velocity Profiles -- Configurations 1, 2, and 3	41
VIII	Boundary-Layer Velocity Profiles -- Configurations 4, 5, and 6	42
IX	Boundary-Layer Velocity Profiles -- Configurations 7, 8, and 9	43
X	Boundary-Layer Velocity Profiles -- Configurations 10, 11, and 12	44
XI	Boundary-Layer Velocity Profiles -- Configurations 13, 14, and 15	45
XII	Boundary-Layer Velocity Profiles -- Configurations 16, 17, and 18	46
XIII	Boundary-Layer Velocity Profile -- Configuration 19	47
XIV	Universal Planar Boundary-Layer Parameters	48

List of Figures

<u>Figure No.</u>	<u>Caption</u>	<u>Page</u>
1	Schematic of the Axisymmetric Body Mounted in the 1.22-Meter (48-Inch) Diameter Wind Tunnel	49
2	Schematic of the Probe Rake System	50
3	Thick Axisymmetric Boundary Layer	51
4	Law of the Wall for the Bare Body	52
5	Screen Data Curve Fit to the Bare Body by the Law of the Wall, Configurations 0 thru 19	53
6	Velocity Defect Law for the Bare Body	54
7	Velocity Defect Law for Screen Configurations 0, 1, 2, and 3	55
8	Velocity Defect Law for Screen Configurations 0, 4, 5, and 6	56
9	Velocity Defect Law For Screen Configurations 0, 7, 8, and 9	57
10	Velocity Defect Law for Screen Configurations 0, 10, 11, and 12	58
11	Velocity Defect Law for Screen Configurations 0, 13, 14, and 15	59
12	Velocity Defect Law for Screen Configurations 0, 16, 17, 18, and 19	60
13	Equilibrium Velocity Defect Law for Screen Configurations 0, 1, 2, and 3	61
14	Equilibrium Velocity Defect Law for Screen Configurations 0, 4, 5, and 6	62
15	Equilibrium Velocity Defect Law for Screen Configurations 0, 7, 8, and 9	63
16	Equilibrium Velocity Defect Law for Screen Configurations 0, 10, 11, and 12	64
17	Equilibrium Velocity Defect Law for Screen Configurations 0, 13, 14, and 15	65

<u>Figure No.</u>	<u>Caption</u>	<u>Page</u>
18	Equilibrium Velocity Defect Law for Screen Configurations 0, 16, 17, 18, and 19	66
19	Universal Plot of $\bar{\Delta}/\delta$ and \bar{G} for All Screen Configurations	67
20	Effect of Screen Length on Boundary-Layer Thickness Based on the Bare Body	68
21	Effect of Screen Length on the Boundary-Layer Displacement Thickness Based on the Bare Body . .	69
22	Effect of Screen Length on the Boundary-Layer Momentum Thickness Based on the Bare Body	70

Nomenclature

A	constant, slope of the curve defining the law of the wall
B_1	constant, intercept of the curve defining the law of the wall for a smooth surface
B_2	constant, intercept of the curve defining the law of the wall for a rough surface
c_f	skin friction coefficient
G	axisymmetric integral family parameter

$$G = \int_0^{\infty} \left(\frac{U_e - U}{U_\tau} \right)^2 \left(\frac{y}{\Delta} \right) d \left(\frac{y}{\Delta} \right)$$

\bar{G}	planar integral family parameter,
-----------	-----------------------------------

$$\bar{G} = \int_0^{\infty} \left(\frac{U_e - U}{U_\tau} \right)^2 d \left(\frac{y}{\Delta} \right)$$

H	axisymmetric shape factor, $H = \delta^*/\theta$
\bar{H}	planar shape factor, $\bar{H} = \bar{\delta}^*/\bar{\theta}$
k	height of surface roughness
k^+	Reynolds number, $k^+ = kU_\tau/\nu$
L	body length
p	static pressure
R	radial distance from body centerline, defined in Figure 3
R_0	body radius, defined in Figure 3
U	local mean axial velocity
U_e	mean axial velocity at the edge of the boundary layer
U_e'	$0.990 U_e$
U_τ	friction velocity, $U_\tau = (\tau_w/\rho)^{1/2}$
U_∞	axial free stream velocity

U^+	U/U_τ
x	axial distance downstream from the nose
y	distance taken perpendicularly from the wall
y_o	$R_o / \cos \phi$
y^+	Reynolds number, $y^+ = yU_\tau/\nu$
Δ	axisymmetric universal thickness,

$$\Delta = \frac{\delta_o^2}{y_o} \int_0^\infty \frac{U_e^{-U}}{U_\tau} \left(\frac{y}{\delta}\right) d\left(\frac{y}{\delta}\right)$$

$\bar{\Delta}$	planar universal thickness,
----------------	-----------------------------

$$\bar{\Delta} = \delta \int_0^\infty \frac{U_e^{-U}}{U_\tau} d\left(\frac{y}{\delta}\right)$$

β	$\frac{\bar{\delta}^*}{\tau_\omega} \frac{dp}{dx}$
δ	boundary-layer thickness
δ^*	axisymmetric displacement thickness

$$\delta^* = \int_0^\infty \left(1 - \frac{U}{U_e}\right) \frac{R}{R_o} dy = \bar{\delta}^* + \Delta \sqrt{\frac{c_f}{2}}$$

$\bar{\delta}^*$	planar displacement thickness
------------------	-------------------------------

$$\bar{\delta}^* = \int_0^\infty \left(1 - \frac{U}{U_e}\right) dy = \bar{\Delta} \sqrt{\frac{c_f}{2}}$$

θ axisymmetric momentum thickness

$$\begin{aligned}\theta &= \int_0^{\infty} \frac{U}{U_e} \left(1 - \frac{U}{U_e}\right) \frac{R}{R_o} dy \\ &= \bar{\theta} + \Delta \sqrt{\frac{c_f}{2}} \left(1 - \frac{\Delta}{y_o} G \sqrt{\frac{c_f}{2}}\right)\end{aligned}$$

$\bar{\theta}$ planar momentum thickness

$$\bar{\theta} = \int_0^{\infty} \frac{U}{U_e} \left(1 - \frac{U}{U_e}\right) dy = \bar{\Delta} \sqrt{\frac{c_f}{2}} \left(1 - \bar{G} \sqrt{\frac{c_f}{2}}\right)$$

μ fluid dynamic viscosity

ν fluid kinematic viscosity

ρ fluid density

τ_w wall shear stress

ϕ angle between body surface and axial direction, defined in Figure 3

Introduction

The results presented in this report document the effects on the boundary layer of an axisymmetric aerodynamic body by the addition of surface roughening screens near the nose. While this method has been applied in the past, the method of achieving the desired results was by trial-and-error of additional surface roughness. Since the results of these efforts were not sufficiently documented, each time a different specific boundary-layer velocity profile was desired the trial-and-error process was repeated. This report will document the results of air tunnel tests on three different mesh size screens of varying length and position on an axisymmetric body in order to build a data base for selecting screens to produce a desired boundary-layer profile shape.

General Characteristics of Turbulent Boundary Layers

From experimental observations, a turbulent boundary layer may be regarded as a composition of layers with an inner and outer region [1]. The existence of the two regions is due to the difference in response of the fluid to the local forces in the two regions. Near the wall, in the viscous part of the profile, the shear velocity and pressure gradient are the dominant parameters. The outer part of the profile depends on the Reynolds stress, hence the two regions require different length scales.

When an obstacle, such as a trip wire or a length of screen is placed near the wall in a turbulent boundary layer the effect of the disturbance disappears in a short distance downstream due to the highly diffuse nature of the flow. The inner part of the velocity profile returns more quickly to a normal profile shape than the outer part [1]. This suggests that the flow close to the wall is relatively insensitive to the flow conditions away from the wall.

Cebeci and Smith [1] explained the results for flow moving from a rough surface to a smooth surface by the variation of the shearing stress distribution in the turbulent boundary layer. As they described it, the shearing stress near the wall very rapidly assumes the new value corresponding to the local surface conditions, while in layers away from the wall the shearing stress equalled the Reynolds stress and changed very slowly. With these effects, a new state of equilibrium was established only at long distances downstream from the start of the rough surface.

From these observations, it is fundamentally impossible to describe the flow in the entire boundary layer in terms of one single set of parameters. For that reason, it is necessary to treat a turbulent boundary layer as a composite of an inner region and an outer region. From the wall the inner region consists of the viscous sublayer, the transitional region or buffer layer, and the fully turbulent region; the inner region extends over approximately 10 - 20% of the boundary-layer thickness. The outer region of the boundary layer contains the remainder of the fluid.

Clauser [2] made extensive surveys of the development of a turbulent boundary layer along the wall of a two-dimensional wind tunnel with and without adverse pressure gradients. He found the boundary layer depended

not only upon local conditions, such as the local values of the pressure gradient, the wall shear stress, the surface roughness, the boundary-layer thickness, but also upon a large portion of the past history of the static pressure gradient. Since the forces acting on a boundary layer are small and the layers are thin, the pressure forces that act upon an effective area across the face of the layer are also very small. With these minute forces present, the boundary layer reacts slowly to a changing environment. Therefore, the past history of the static pressure gradient plays an important part in the boundary layer's downstream development.

If the measured velocities are nondimensionalized by the friction velocity, U_τ , then all constant pressure turbulent profiles are similar. Even with large roughness elements good agreement with the velocity defect law should be expected with the same pressure history. Clauser [2] showed that two distinct pressure histories produced two separate velocity profiles when plotted by the velocity defect law. Each profile produced a single curve with little data scatter, thus indicating that they were nearly identical members of an equilibrium set of profiles.

Inner Region Over a Smooth Two-Dimensional Surface. The mean velocity distribution in this region is generally assumed to be determined by the wall shear stress τ_w , the fluid density ρ , the fluid viscosity μ , and the distance y from the wall. It is given by the following expression known as the law of the wall:

$$U^+ \equiv U/U_\tau = A \ln y^+ + B_1 \quad (1)$$

where U is the mean velocity and A and B_1 are constants. The factor U_τ is called the friction velocity and is defined as

$$U_\tau = (\tau_w/\rho)^{1/2} \quad (2)$$

The parameter y^+ is a Reynolds number based on typical velocity and length scales for the turbulence in the inner region and is defined as

$$y^+ = y U_\tau/\nu \quad (3)$$

where y is the distance from the wall and ν is the kinematic viscosity.

Inner Region Over a Rough Two-Dimensional Surface. From the discussion in the preceding sections we know surface roughness effects only the inner region. On the other hand, the surface may be considered aerodynamically smooth for a turbulent boundary layer if the height of the roughness elements, k , is less than the thickness of the viscous sublayer. Since in most cases the viscous sublayer is extremely thin, the roughness elements must be very small for the surface to be aerodynamically smooth. On a large body, as the boundary-layer thickness and its Reynolds number changes, the surface may change from rough to aerodynamically smooth.

From experiments and dimensional analysis in the fully turbulent part of the inner region, the law of the wall for a surface with uniform roughness is given by the expression

$$U^+ = A \ln y^+ + B_2(k^+) \quad (4)$$

where A is expected to be the same as for a smooth surface. B_2 is a function of k^+ , the roughness Reynolds number defined by

$$k^+ = kU_\tau/\nu \quad (5)$$

where k is the roughness height.

Outer Region of a Two-Dimensional Boundary Layer. The outer region of the turbulent boundary layer extends over 80 - 90% of the boundary-layer thickness. From experimental results, the mean velocity distribution in this region can be described by the following expression, called the velocity-defect law:

$$(U_e - U)/U_\tau = f(y/\delta) \quad (6)$$

where U_e is the velocity at the edge of the boundary layer and δ is the boundary-layer thickness. Equation (6) is not valid near the wall, since the viscosity becomes important there and the flow must depend on a Reynolds number ($\delta U_\tau/\nu$) as well as the ratio y/δ . On the other hand, at the edge of the boundary layer, y approaches δ and the function $f(y/\delta)$ goes to zero. In addition, the function f may be affected by a streamwise pressure gradient and therefore would also depend on x .

Axisymmetric Bodies. Patel, Nakayama, and Damian [3] have shown that thick axisymmetric boundary-layer velocity profiles could deviate appreciably from the two-parameter families of shape factor and Reynolds number constructed primarily for thin two-dimensional boundary layers. Use of integral parameters will not lead to improved velocity profile relations that are better than the usual plane surface boundary-layer definitions.

Parameters for Analysis

For an axisymmetric body with screens the question arises as to what parameters can be used to analyze the data that have been obtained. Certainly the screen parameters of mesh size and screen length should be used. Boundary-layer parameters should include the boundary-layer thickness, planar and axisymmetric displacement and momentum thicknesses. In addition, the skin friction coefficient and pressure gradient could be of some use. Clauser [2] defined two additional parameters that were independent of the Reynolds number and roughness. He defined a simple universal thickness for a two-dimensional flow as:

$$\bar{\Delta} = \int_0^{\infty} \left(\frac{U_e - U}{U_{\tau}} \right) dy = \delta \int_0^{\infty} \left(\frac{U_e - U}{U_{\tau}} \right) d \left(\frac{y}{\delta} \right) \quad (7)$$

A second parameter, similar to the shape factor, H, was defined as

$$\bar{G} = \int_0^{\infty} \left(\frac{U_e - U}{U_{\tau}} \right)^2 d \left(\frac{y}{\Delta} \right) = \int_0^{\infty} \left(\frac{U_e - U}{U_{\tau}} \right)^2 dy / \int_0^{\infty} \left(\frac{U_e - U}{U_{\tau}} \right) dy \quad (8)$$

The derivation of the axisymmetric displacement thickness in terms of c_f , $\bar{\Delta}$ and Δ is given in Appendix A and can be written as

$$\begin{aligned} \delta^* &= \sqrt{\frac{c_f}{2}} \Delta + \bar{\delta}^* \\ &= \sqrt{\frac{c_f}{2}} (\Delta + \bar{\Delta}) \end{aligned} \quad (9)$$

where

$$\overline{\delta^*} = \text{planar displacement thickness, } \overline{\Delta} \sqrt{\frac{c_f}{2}}$$

$$\delta = \text{boundary-layer thickness}$$

$$y_o = R_o / \cos \phi \text{ defined in Figure 3}$$

$$c_f = \text{shear stress coefficient}$$

$$\Delta = \frac{\delta^2}{y_o} \int_0^{\infty} \left(\frac{U_e - U}{U_\tau} \right) \left(\frac{y}{\delta} \right) d \left(\frac{y}{\delta} \right)$$

and

$$\overline{\Delta} = \delta \int_0^{\infty} \left(\frac{U_e - U}{U_\tau} \right) d \left(\frac{y}{\delta} \right)$$

Using a similar derivation in Appendix B the momentum thickness for an axisymmetric body may be obtained and is given by the following expression:

$$\theta = \overline{\theta} + \Delta \sqrt{\frac{c_f}{2}} \left(1 - \frac{\Delta}{y_o} G \sqrt{\frac{c_f}{2}} \right) \quad (10)$$

where

$$\overline{\theta} = \text{planar momentum thickness, } \overline{\Delta} \sqrt{\frac{c_f}{2}} \left(1 - \overline{G} \sqrt{\frac{c_f}{2}} \right)$$

and

$$G = \int_0^{\infty} \left(\frac{U_e - U}{U_\tau} \right)^2 \left(\frac{y}{\Delta} \right) d \left(\frac{y}{\Delta} \right)$$

From the derivation in Appendix C the axisymmetric shape factor is given by

$$H = \frac{\bar{\Delta} + \Delta}{\bar{\Delta} \left(1 - \bar{G} \sqrt{\frac{c_f}{2}} \right) + \Delta \left(1 - G \frac{\Delta}{y_0} \sqrt{\frac{c_f}{2}} \right)} \quad (11)$$

Instrumentation and Data Acquisition

These tests were conducted in the 1.22-meter (48-inch) diameter wind tunnel in the Fluids Engineering Department of the Applied Research Laboratory, The Pennsylvania State University. An axisymmetric body, with a length to diameter ratio of 8.794, was used for this experimental program. The model was mounted in the tunnel with three MacWhyte struts, which are aerodynamically shaped to reduce flow distortions. One strut was located in the vertical plane at $x/L=0.2298$. At the same location a wire was stretched from each side of the body to the tunnel walls in the horizontal plane. Two additional struts were located at $x/L=0.5314$, each at 45° to the vertical. The placement of the screens was just aft of the forward MacWhyte strut. The flow velocity at the edge of the boundary layer in the measuring plane was 24.38 m/sec (80 ft/sec). Measurements were made in a plane located at $x/L=0.972$, on the body. Figure 1 is a sketch of the model installation. A liner was used in the test section to eliminate any effects produced by tunnel wall interference.

The boundary-layer velocity measurements were obtained by a stationary pitot-static tube and a rotating rake system comprised of total and static pressure tubes. A schematic of the rake system is shown in Figure 2. Note there were three total pressure tube rakes and one

static pressure tube rake. With the combination of these rakes, local axial velocity was calculated. A traversing motor and scanivalve for the rake were mounted inside the model; the electrical leads and common pressure tube were fed from the aft end of the model to the outside of the tunnel through a metal tube. A stationary pitot-static probe was positioned 10.16 cm (4.00 inch) from the body surface in the plane of rotation of the rakes. A second stationary pitot-static probe was mounted 12.70 cm (5.00 inch) from the liner surface in the same plane as the rakes; this sensor measured the free stream velocity in the test section. In addition, an electronic thermometer measured the air temperature in the settling section of the wind tunnel.

The data acquisition system is shown schematically in Figure 1. The common pressure tube from a Scanivalve was connected to a differential pressure transducer; the resultant electrical signal was fed to a micro-processor data acquisition system which then sent all inputs to a paper tape punch for a permanent record and later data reduction. The tunnel static pressure was used as the reference pressure. The fixed boundary-layer pitot-static tube was connected to a micro-manometer; velocity measurements from this probe were calculated from the readings. The free stream pitot-static probe tube connections were attached to a second differential pressure transducer and the electrical signal again fed to the micro-processor.

Screens

The type of screens chosen for this study had the following description:

	Mesh	Wire Diameter		Open Area (%)	Type of Weave
		cm	Inch		
(1)	4	0.0635	(0.025)	81	Double Intermediate Crimp
(2)	10	0.0508	(0.020)	64	Plain Crimp
(3)	16	0.0406	(0.016)	55.4	Plain Crimp

The mesh number refers to the number of open spaces between the wires in a piece of screen 2.54 cm (1.00 inch) long. The screens were made to completely encircle the model and provide a 0.635 cm (0.25 inch) overlap when installed. A list of the screen test configurations is shown in Table I. Three screens were made for each mesh size; two screens 15.24 cm (6 inch) in width and one 30.48 cm (12 inch) wide screen were made. This provides for screen combinations of 15.24, 30.48, 45.72 and 60.96 cm widths or equivalently 6, 12, 18 and 24 inch widths. Each screen had two 0.9525 cm (0.375 inch) wide metal bands soldered along the edges; each band was 0.0396875 cm (0.015625 inch) thick. Hose clamps were soldered to the ends of the bands to facilitate quick and easy exchange of the screens during the tests. During the tests the screw mechanism of the hose clamp disturbed the flow enough to render three data points at the downstream location useless.

Test Procedure

The procedure involved in acquiring the data was relatively simple. A screen was attached to the model, the tunnel flow velocity brought up to 24.38 m/sec (80 ft/sec) then the micro-processor automatically stepwise incremented the traversing rakes through 360° in 18° increments; this action produced 20 data points for each probe radius. The micro-processor electronically controlled the sequence of data acquisition. This included the activation of the scanivalve movement for pressure recordings, free stream flow velocity recordings, temperature recordings,

and movement of the traversing motor. The stationary pitot-static probe located 10.16 cm (4 inch) from the model surface was connected to a micromanometer. The readings from the manometer were taken by hand during the traverse of the rotating probe.

Data Analysis

The data tapes from the tape punch machine were converted to computer cards and reduced by a series of computer programs. A plotting program displayed the circumferential survey data at each radius; bad data points were then eliminated from the data set and the remaining points averaged. This provided a circumferentially averaged velocity profile which was later plotted by hand.

It was discovered that an insufficient number of data points had been taken to completely define the velocity profile in the outer part of the boundary layer. By the use of the boundary-layer similarity laws, the law of the wall and the velocity defect law, the limited profile data was extended to completely define the profile shape.

With no roughness added the data near the wall was matched to Billet's [4] data using the law of the wall, $U^+ = A \log y^+ + B_1$. Figure 4 shows these. His data was used as a basis to determine the values of A and B_1 (refer to Equation (1)). Since both U^+ and y^+ are functions of U_τ , it required an iteration process to match data sets and determine the value of U_τ . The expression for the law of the wall, used to match the data, is given as follows:

$$U^+ = 9.9515 \log_{10} y^+ - 3.9331 \quad . \quad (12)$$

Figure 5 shows the screen data curve fit to the bare body data using Equation (12).

It is immediately apparent that the coefficients, A and B_1 , in Equation (12) do not match the values of $A = 5.75$ and $B_1 = 5.5$ commonly associated with the law of the wall. An explanation for a similar deviation from the law of the wall in pipe flow was discussed by Patel [5]. Patel observed that in both adverse and favorable pressure gradients the departure of the velocity distribution from the law of the wall in the initial stages was gradual. Comparison of adverse pressure gradient profiles with the constant pressure boundary-layer profile showed that the application of pressure gradients reduces the extent of the region in which the law of wall is valid, or follows the 5.75 slope of the law of the wall curve. This process continues until at some large value of the pressure gradient the straight line portion is absent altogether. It is this adverse pressure gradient plus the fact that the wall shear stress is going to zero at the aft end of the axisymmetric body, that produced this deviation in the curve of the law of the wall.

Once the value of U_τ was determined the outer part of the boundary-layer velocity profile could be matched. This was accomplished by using the velocity defect law $(U_e' - U)/U_\tau = f(y/\delta)$, refer to Equation (6). Here, U_e' was taken to be 0.990 times the velocity outside the boundary layer, U_e since δ was defined at $0.99 U_e$. Again, an iteration was required to determine the value of δ . Figure 6 shows the data for the body without screens plotted by the velocity defect law. Note in this figure the largest discrepancy between Billet's [4] data and these data was 4.1%. Both sets of data were taken from the same model with the same probe system.

All things considered, the same flow conditions and pressure gradient should have been reproduced.

The data obtained with the screens on the body were plotted to conform to the velocity defect law. Here, some subjective judgement entered into the data analysis. It was found that matching one portion of the screen data to the data without the screens installed resulted in a curve with an abnormal shape (high curvature in the middle). The explanation for these differences is the static pressure gradient along the body. For each screen configuration the pressure gradient was different. This was due to the different boundary-layer thicknesses and the blockage effect. Clauser [2] showed what to expect with different pressure gradients. So, following Clauser [2] the velocity defect law was replotted to produce a smooth curve that approximated the shape of the curve for the bare body. This technique was used to iterate on δ until the curve appeared smooth. Figures 7 through 12 show the results of this data analysis process.

With all the velocity profile parameters defined by the law of the wall and the velocity defect law the missing portions of the velocity profiles were obtained. At this point in the analysis the shape of the profile was defined, U/U_e vs y , and δ was estimated.

To carry the analysis a little further, Clauser's planar parameters, $\bar{\Delta}$ and \bar{G} , for equilibrium boundary layers were calculated, refer to Equations (7) and (8), respectively. Next the velocity defect law was plotted for equilibrium boundary layers, $U-U_e'/U_\tau$ vs $y/\bar{\Delta}$, as shown in Figures 13 thru 18. Clauser [2] observed that boundary layers with a constant value of $\beta = \delta^*/\tau_\omega dp/dx$ had a unique curve when plotted in such a manner. As shown in these figures, β was not constant for any

of the screen configurations. However, some configurations had nearly identical curves. These pairs include the following screen configurations:

- (1) 0 and 7
- (2) 1 and 5
- (3) 8 and 12 .

The change in curve shape from one screen configuration to another is attributed to the changes in the static pressure gradient along the body due to the different growth rates and thicknesses of the boundary layer. By plotting $\bar{\Delta}/\delta$ vs \bar{G} for each screen configuration as shown in Figure 19, the result was a straight line taking the following form

$$\frac{\bar{\Delta}}{\delta} = 0.7988 \bar{G} - 2.748 \quad (13)$$

where $\bar{\Delta}$ and \bar{G} are defined by Equations (7) and (8), respectively. This figure shows the relative effect of the β term or pressure gradient, lower values of \bar{G} and $\bar{\Delta}/\delta$ indicate a more favorable (decreasing) pressure gradient.

Results

The results of this study are presented in Tables I thru XIV and Figures 20, 21 and 22. Table I lists all the screen configurations, including the mesh size, screen length, and screen location.

The planar boundary-layer characteristics are listed in Table II. These parameters include the boundary-layer thickness, displacement and momentum thicknesses, and shape factor. In a similar manner the axisymmetric boundary-layer characteristics are listed in Table III. Table IV

lists the following skin friction parameters for the various screen configurations: friction velocity, skin friction coefficient, and wall shear stress. Now, Table V shows the effects of the screen configurations on the boundary-layer characteristics. Essentially, this table shows the percentage change in the boundary-layer parameter for each screen configuration, based on bare body results. The results presented in this table were derived from Tables II and III; these results are also plotted in Figures 20, 21 and 22. In these figures the changes in parameters were plotted as a function of screen length.

Figure 20 shows the effects of screen length and mesh size on boundary-layer thickness. Screens with mesh size 4 had the greatest impact, followed by mesh sizes 10 and 16. Similarly, the same trend appears in Figures 21 and 22 for the change in displacement and momentum thickness, respectively. In each of these figures percentage change in boundary-layer parameter is based on the value obtained from the bare body. From these figures the effects of the screens with mesh size 16 tend to be lower and the rate of change with increasing length tends to be less than the other mesh sizes. This is probably due to the smaller wire diameter and its relation to the thickness of the laminar sublayer. Since these wires do not protrude as far above the sublayer as the other mesh size wires, the smaller wires have less effect on the flow outside the sublayer.

Use of the Screen Data

To modify the boundary layer on an axisymmetric body and achieve a prescribed profile shape the following procedure is proposed.

- (1) The boundary layer on the body without the added roughness should be measured along with the body surface static pressure in the region of interest. This bare body data is the base to which the added surface roughness will be applied.
- (2) The momentum and displacement thicknesses can then be calculated from the base boundary-layer velocity profile. In addition, the pressure gradient and $\beta = \frac{\overline{\delta^*}}{\tau_w} \frac{dp}{dx}$, can also be computed.
- (3) From the desired velocity profile the momentum and displacement thicknesses can be computed. If the pressure gradient is known, β can also be calculated.
- (4) Now, the percentage difference in momentum and displacement thicknesses between the bare body profile and the desired profile can be calculated using the following expressions:

$$\Delta\delta^* = \frac{\delta_{\text{desired}}^* - \delta_{\text{base}}^*}{\delta_{\text{base}}^*} \times 100$$

$$\Delta\theta = \frac{\theta_{\text{desired}} - \theta_{\text{base}}}{\theta_{\text{base}}} \times 100 .$$

- (5) The screen data can now be used to select the type and length of screen needed to obtain the calculated change in the boundary-layer parameters. Using the calculated $\Delta\delta^*$ and $\Delta\theta$ the type of screen (mesh size) and estimated length are obtained from Figures 21 and 22, respectively.
- (6) Attach the chosen screen to the model and measure the resulting boundary layer
- (7) The shape of the profile may be changed by moving a length of screen farther back from the nose; this produces a fuller profile

shape near the wall. The data in Tables VI through XIII show that small changes in the profile shape may be made by moving a length of screen towards the aft end of the model. Using the data in these tables small changes may be estimated.

Conclusions

From the results of this test program the following conclusions are drawn:

- (1) Small mesh sizes with large wire diameters produce greater effects on the boundary-layer parameters than large mesh sizes with smaller wire diameters for a given length of screen.
- (2) Increasing the screen length also increases the boundary layer growth.
- (3) This body shape has a universal curve for the boundary layer which is dependent on the axial static pressure gradient and wall shear stress, see Figure 19.

Recommendations

From the results of this test program and from the method and test procedures used, the following recommendations are made:

- (1) Boundary-layer velocity surveys should be made to the edge of the boundary layer and beyond. A traversing probe system would be better than a fixed probe system. This would completely define the velocity profile and explicitly give the boundary-layer thickness.
- (2) Static pressure measurements should be made along the surface of the body in the region of the velocity survey. This would allow the determination of the axial static pressure gradient. Knowing this pressure gradient is important since it effects the characteristics of the law of the wall and would help in under-

24 March 1978
BER:jep

standing the development of the boundary layer if it should deviate from normal.

References

- [1] Cebeci, T. and Smith, A. M. O., Analysis of Turbulent Boundary Layers, Academic Press, New York, 1974.
- [2] Clauser, F. H., "Turbulent Boundary Layers in Adverse Pressure Gradients," Journal of Aeronautical Sciences, Vol. 21, pp. 91-108, 1954.
- [3] Patel, V. C., Nakayama, A., and Damian, R., "An Experimental Study of the Thick Turbulent Boundary Layer Near the Tail of a Body of Revolution," Iowa Institute of Hydraulic Research, Report 142, 1973.
- [4] Billet, M. L., "Rotor Incoming Velocity Profile Measurements," Applied Research Laboratory Technical Memorandum, File No. 76-254, October 1976.
- [5] Patel, V. C., "Calibration of the Preston Tube and Limitations on Its Use in Pressure Gradients," Journal of Fluid Mechanics, Vol. 23, Part 1, pp. 185-208, 1965.
- [6] Ludwig, H. and Tillmann, W., "Investigations of the Wall Shearing Stress in Turbulent Boundary Layers," NACA TM No. 1285, 1950.

Appendix A: Derivation of the Axisymmetric Displacement Thickness

The axisymmetric displacement thickness is defined as follows:

$$\delta^* = \int_0^{\infty} (1 - U/U_e) R/R_o dy \quad (A-1)$$

where U is the streamwise velocity, U_e is the velocity at the edge of the boundary layer, R is the radial location of velocity U from the centerline, R_o is the body radius where the velocity profile is defined, and y is the normal distance from the body surface as shown in Figure 3.

Ludwig and Tillmann [6] showed that near a two-dimensional smooth wall the mean velocity data points fall on the well known curve of the law of the wall (U/U_τ vs yU_τ/ν), even in a static pressure gradient. It has been shown that the following method of calculating shear stress can be used: $U/U_\tau = U/U_e \sqrt{2/c_f}$ and $yU_\tau/\nu = yU_e/\nu \sqrt{c_f/2}$.

Rearranging the terms in these expressions we have

$$\frac{U}{U_e} = \frac{U}{U_\tau \sqrt{2/c_f}}$$

thus

$$U_e = U_\tau \sqrt{2/c_f} \quad (A-2)$$

Equation (A-1) can be expanded and Equation (A-2) substituted for the appropriate term to yield

$$\begin{aligned}
 \delta^* &= \int_0^{\infty} \left(\frac{U_e - U}{U_e} \right) \frac{R}{R_o} dy \\
 &= \int_0^{\infty} \left(\frac{U_e - U}{U_{\tau} \sqrt{2/c_f}} \right) \frac{R}{R_o} dy \\
 &= \sqrt{c_f/2} \int_0^{\infty} \left(\frac{U_e - U}{U_{\tau}} \right) \frac{R}{R_o} dy \quad . \quad (A-3)
 \end{aligned}$$

From Figure 1 we have

$$R = (y+y_o) \cos\phi$$

and

$$R_o = y_o \cos\phi$$

therefore

$$\frac{R}{R_o} = \frac{(y+y_o) \cos\phi}{y_o \cos\phi} = \frac{y+y_o}{y_o} \quad . \quad (A-4)$$

Substitution of Equation (A-4) into Equation (A-3) we have

$$\delta^* = \sqrt{c_f/2} \int_0^{\infty} \left(\frac{U_e - U}{U_{\tau}} \right) \left(\frac{y+y_o}{y_o} \right) dy \quad . \quad (A-5)$$

By changing the variable of integration in Equation (A-5) we have

$$\delta^* = \sqrt{c_f/2} \delta \int_0^{\infty} \left(\frac{U_e - U}{U_{\tau}} \right) \left[\frac{(y/\delta)}{(y_o/\delta)} + 1 \right] d(y/\delta) \quad . \quad (A-6)$$

The integral in Equation (A-6) can be expanded to yield

$$\begin{aligned} \delta^* = & \delta \sqrt{c_f/2} \int_0^\infty \left(\frac{U_e - U}{U_\tau} \right) \frac{(y/\delta)}{(y_o/\delta)} d(y/\delta) \\ & + \delta \sqrt{c_f/2} \int_0^\infty \left(\frac{U_e - U}{U_\tau} \right) d(y/\delta) \end{aligned} \quad (A-7)$$

The second term in Equation (A-7) is Clauser's [2] expression for the planar displacement thickness, $\overline{\delta^*} = \sqrt{c_f/2} \overline{\Delta}$, where $\overline{\Delta} = \delta \int_0^\infty (U_e - U/U_\tau) d(y/\delta)$ so we have

$$\delta^* = \frac{\delta^2}{y_o} \sqrt{c_f/2} \int_0^\infty \left(\frac{U_e - U}{U_\tau} \right) \left(\frac{y}{\delta} \right) d(y/\delta) + \overline{\delta^*} \quad (A-8)$$

By defining Δ for the axisymmetric case in the following manner

$$\Delta = \frac{\delta^2}{y_o} \int_0^\infty \left(\frac{U_e - U}{U_\tau} \right) \left(\frac{y}{\delta} \right) d(y/\delta) \quad (A-9)$$

we have

$$\delta^* = \sqrt{c_f/2} \Delta + \overline{\delta^*} \quad (A-10)$$

Appendix B: Derivation of the Axisymmetric Momentum Thickness

The axisymmetric momentum thickness is defined as follows:

$$\theta = \int_0^{\infty} U/U_e (1 - U/U_e) R/R_o dy \quad . \quad (B-1)$$

The first term inside the integral sign in Equation (B-1) may be expanded by adding and subtracting 1 as follows:

$$\theta = \int_0^{\infty} \left(\frac{U}{U_e} - \frac{U_e}{U_e} + 1 \right) \left(\frac{U_e - U}{U_e} \right) \frac{R}{R_o} dy \quad . \quad (B-2)$$

Then the terms in Equation (B-2) may be recombined as follows:

$$\begin{aligned} \theta &= \int_0^{\infty} \left(\frac{U - U_e}{U_e} + 1 \right) \left(\frac{U_e - U}{U_e} \right) \frac{R}{R_o} dy \\ &= \int_0^{\infty} \left(1 - \frac{U_e - U}{U_e} \right) \left(\frac{U_e - U}{U_e} \right) \frac{R}{R_o} dy \\ &= \int_0^{\infty} \left(\frac{U_e - U}{U_e} \right) \frac{R}{R_o} dy - \int_0^{\infty} \left(\frac{U_e - U}{U_e} \right)^2 \frac{R}{R_o} dy \quad . \quad (B-3) \end{aligned}$$

Immediately, the first term in Equation (B-3) is recognized as the axisymmetric displacement thickness δ^* . In the second term substitution of $U_e = U_\tau \sqrt{2/c_f}$ and $R/R_o = (y+y_o)/y_o$ yields the following expression

$$\theta = \delta^* - \int_0^{\infty} \left(\frac{U_e - U}{\sqrt{2/c_f} U_\tau} \right)^2 \left(\frac{y+y_o}{y_o} \right) dy$$

$$\theta = \delta^* - \frac{c_f}{2} \int_0^{\infty} \left(\frac{U_e - U}{U_\tau} \right)^2 \left(\frac{y}{y_0} + 1 \right) dy \quad . \quad (B-4)$$

By changing the variable of integration in Equation (B-4) we find

$$\begin{aligned} \theta &= \delta^* - \frac{c_f}{2} \int_0^{\infty} \left(\frac{U_e - U}{U_\tau} \right)^2 \frac{y}{y_0} dy - \frac{c_f}{2} \int_0^{\infty} \left(\frac{U_e - U}{U_\tau} \right)^2 dy \\ &= \delta^* - \frac{\Delta^2}{y_0} \frac{c_f}{2} \int_0^{\infty} \left(\frac{U_e - U}{U_\tau} \right)^2 \left(\frac{y}{\Delta} \right) d\left(\frac{y}{\Delta} \right) - \frac{\bar{\Delta} c_f}{2} \int_0^{\infty} \left(\frac{U_e - U}{U_\tau} \right)^2 d\left(\frac{y}{\Delta} \right) \quad . \quad (B-5) \end{aligned}$$

Now, by defining

$$\bar{G} = \int_0^{\infty} \left(\frac{U_e - U}{U_\tau} \right)^2 d\left(\frac{y}{\Delta} \right)$$

and

$$G = \int_0^{\infty} \left(\frac{U_e - U}{U_\tau} \right)^2 \left(\frac{y}{\Delta} \right) d\left(\frac{y}{\Delta} \right) \quad .$$

Equation (B-5) reduces to the following expression

$$\theta = \delta^* - \frac{\Delta^2}{y_0} \frac{c_f}{2} G - \bar{\Delta} \frac{c_f}{2} \bar{G} \quad . \quad (B-6)$$

Now, by replacing δ^* in Equation (B-6) by Equation (A-10) and Clauser's expression for the planar displacement thickness, $\bar{\delta}^* = \sqrt{c_f/2} \bar{\Delta}$, then rearranging terms we have

$$\begin{aligned}
\theta &= \sqrt{c_f/2} \Delta + \sqrt{c_f/2} \bar{\Delta} - \frac{\Delta^2 c_f}{y_o} \frac{G}{2} - \bar{\Delta} \frac{c_f}{2} \bar{G} \\
&= \sqrt{c_f/2} \bar{\Delta} - \bar{\Delta} \frac{c_f}{2} \bar{G} + \sqrt{c_f/2} \Delta - \frac{\Delta^2 c_f}{y_o} \frac{G}{2} \\
&= \sqrt{c_f/2} (1 - \bar{G} \sqrt{c_f/2}) \bar{\Delta} + \sqrt{c_f/2} (1 - \frac{\Delta}{y_o} G \sqrt{c_f/2}) \Delta \quad . \quad (B-7)
\end{aligned}$$

The first term in Equation (B-7) is recognized as Clauser's derivation for the planar momentum thickness $\bar{\theta}$, therefore we have

$$\theta = \bar{\theta} + \sqrt{c_f/2} (1 - \frac{\Delta}{y_o} G \sqrt{c_f/2}) \Delta \quad . \quad (B-8)$$

Appendix C: Derivation of the Axisymmetric Shape Factor

The axisymmetric shape factor is defined as

$$H = \delta^*/\theta \quad (C-1)$$

By substituting in the expressions for the axisymmetric displacement and momentum thicknesses given by Equations (A-10) and (B-8), respectively, we have

$$H = \frac{\Delta \sqrt{c_f/2} + \bar{\delta}^*}{\bar{\theta} + \sqrt{c_f/2} \left(\Delta - \frac{\Delta^2}{y_o} G \sqrt{c_f/2} \right)} \quad (C-2)$$

By substituting in the expressions for $\bar{\delta}^*$ and $\bar{\theta}$ given in Appendices A and B respectively we have

$$\begin{aligned} H &= \frac{\Delta \sqrt{c_f/2} + \bar{\Delta} \sqrt{c_f/2}}{\bar{\Delta} \sqrt{c_f/2} (1 - \bar{G} \sqrt{c_f/2}) + \sqrt{c_f/2} \left(\Delta - \frac{\Delta^2}{y_o} G \sqrt{c_f/2} \right)} \\ &= \frac{\Delta + \bar{\Delta}}{\bar{\Delta} - \bar{\Delta} \bar{G} \sqrt{c_f/2} + \Delta - \frac{\Delta^2}{y_o} G \sqrt{c_f/2}} \\ &= \frac{\Delta + \bar{\Delta}}{\Delta + \bar{\Delta} - \sqrt{c_f/2} (\bar{\Delta} \bar{G} - \frac{\Delta^2}{y_o} G)} \quad (C-3) \end{aligned}$$

Table I
Screen Configurations

Configuration No.	Mesh Size	Screen Length		Screen Location (x/L)
		cm	(in.)	
0	----	-----	-----	-----
1	4	15.240	(6)	0.2298
2	4	30.480	(12)	0.2298
3	4	60.960	(24)	0.2298
4	10	15.240	(6)	0.2298
5	10	30.480	(12)	0.2298
6	10	60.960	(24)	0.2298
7	16	15.240	(6)	0.2298
8	16	30.480	(12)	0.2298
9	16	60.960	(24)	0.2298
10	4	30.480	(12)	0.3160
11	4	30.480	(12)	0.4452
12	10	30.480	(12)	0.4452
13	4	30.480	(12)	0.2298
	10	30.480	(12)	0.3160
14	4	30.480	(12)	0.2298
	16	30.480	(12)	0.3160
15	4	30.480	(12)	0.2298
	10	30.480	(12)	0.3160
	16	30.480	(12)	0.4022
16	4	45.720	(18)	0.2298
	10	30.480	(12)	0.3591
	16	30.480	(12)	0.4452
17	4	15.240	(6)	0.4452
18	10	30.480	(12)	0.2298
	4	30.480	(12)	0.3160
19	16	30.480	(12)	0.2298
	4	30.480	(12)	0.3160

Table II
Planar Boundary-Layer Characteristics

Configuration No.	δ		$\overline{\delta^*}$		$\overline{\theta}$		\overline{H}
	cm	(in.)	cm	(in.)	cm	(in.)	
0	11.200	(4.410)	2.964	(1.167)	1.758	(0.692)	1.686
1	12.652	(4.981)	3.139	(1.236)	1.933	(0.761)	1.624
2	13.848	(5.452)	3.287	(1.294)	2.062	(0.812)	1.593
3	15.199	(5.984)	3.432	(1.351)	2.194	(0.864)	1.564
4	12.256	(4.825)	3.134	(1.234)	1.897	(0.747)	1.652
5	12.817	(5.046)	3.175	(1.250)	1.951	(0.768)	1.626
6	14.526	(5.719)	3.398	(1.338)	2.144	(0.844)	1.585
7	12.118	(4.771)	3.170	(1.248)	1.887	(0.743)	1.680
8	12.733	(5.013)	3.195	(1.258)	1.940	(0.764)	1.645
9	13.523	(5.324)	3.259	(1.283)	2.022	(0.796)	1.613
10	13.249	(5.216)	3.139	(1.236)	1.958	(0.771)	1.603
11	12.987	(5.113)	3.210	(1.264)	1.981	(0.780)	1.620
12	12.489	(4.917)	3.165	(1.246)	1.925	(0.758)	1.644
13	15.037	(5.920)	3.485	(1.372)	2.207	(0.869)	1.579
14	14.288	(5.625)	3.370	(1.327)	2.121	(0.835)	1.590
15	15.977	(6.290)	3.635	(1.431)	2.299	(0.905)	1.581
16	15.215	(5.990)	3.520	(1.386)	2.220	(0.874)	1.587
17	12.817	(5.046)	3.134	(1.234)	1.923	(0.757)	1.629
18	18.618	(7.330)	3.942	(1.552)	2.591	(1.020)	1.521
19	14.961	(5.890)	3.411	(1.343)	2.159	(0.850)	1.579

Table III
Axisymmetric Boundary-Layer Characteristics

Configuration No.	δ^*		θ		H
	cm	(in.)	cm	(in.)	
0	6.825	(2.687)	4.529	(1.783)	1.507
1	7.874	(3.100)	5.425	(2.136)	1.451
2	8.638	(3.401)	6.078	(2.393)	1.422
3	9.462	(3.725)	6.792	(2.674)	1.393
4	7.732	(3.044)	5.242	(2.064)	1.475
5	8.001	(3.150)	5.578	(2.196)	1.452
6	9.167	(3.609)	6.482	(2.552)	1.414
7	7.752	(3.052)	5.176	(2.038)	1.498
8	7.996	(3.148)	5.448	(2.145)	1.468
9	8.250	(3.248)	5.735	(2.258)	1.438
10	7.828	(3.082)	5.471	(2.154)	1.431
11	8.181	(3.221)	5.659	(2.228)	1.446
12	7.884	(3.104)	5.364	(2.112)	1.469
13	9.370	(3.689)	6.637	(2.613)	1.412
14	9.012	(3.548)	6.347	(2.499)	1.420
15	10.023	(3.946)	7.120	(2.803)	1.408
16	9.700	(3.819)	6.878	(2.708)	1.411
17	7.854	(3.092)	5.430	(2.138)	1.446
18	12.327	(4.853)	9.139	(3.598)	1.349
19	9.271	(3.650)	6.591	(2.595)	1.406

Table IV
Skin Friction Parameters

Configuration No.	U_{τ}		c_f	τ_w	
	m/sec	(ft/sec)		nt/m ²	(lbf/ft ²)
0	0.477	(1.565)	0.0007654	0.2697	(0.005633)
1	0.496	(1.628)	0.0008282	0.2919	(0.006096)
2	0.506	(1.661)	0.0008622	0.3038	(0.006346)
3	0.515	(1.691)	0.0008936	0.3149	(0.006577)
4	0.487	(1.598)	0.0007980	0.2812	(0.005873)
5	0.495	(1.624)	0.0008242	0.2904	(0.006066)
6	0.509	(1.669)	0.0008705	0.3068	(0.006407)
7	0.485	(1.590)	0.0007900	0.2784	(0.005815)
8	0.493	(1.617)	0.0008171	0.2880	(0.006014)
9	0.498	(1.635)	0.0008354	0.2944	(0.006148)
10	0.505	(1.656)	0.0008570	0.3020	(0.006307)
11	0.504	(1.653)	0.0008539	0.3009	(0.006284)
12	0.495	(1.623)	0.0008232	0.2900	(0.006058)
13	0.514	(1.686)	0.0008883	0.3130	(0.006538)
14	0.511	(1.677)	0.0008788	0.3097	(0.006468)
15	0.507	(1.663)	0.0008642	0.3046	(0.006361)
16	0.505	(1.656)	0.0008570	0.3020	(0.006307)
17	0.492	(1.614)	0.0008141	0.2868	(0.005991)
18	0.510	(1.673)	0.0008747	0.3082	(0.006438)
19	0.508	(1.668)	0.0008694	0.3064	(0.006399)

Table V

Effect of Screen Configurations on Boundary-Layer Characteristics

Configuration No.	$\Delta\delta$ (%)	$\overline{\Delta\delta^*}$ (%)	$\overline{\Delta\theta}$ (%)	$\Delta\delta^*$ (%)	$\Delta\theta$ (%)
0	BASE	BASE	BASE	BASE	BASE
1	12.948	5.912	9.971	15.370	19.798
2	23.628	10.883	17.341	26.572	34.212
3	35.692	15.767	24.855	38.630	49.972
4	9.410	5.741	7.948	13.286	15.760
5	14.422	7.112	10.982	17.231	21.649
6	29.682	14.653	21.965	34.313	43.130
7	8.186	6.941	7.370	13.584	14.302
8	13.674	7.798	10.405	17.157	20.303
9	20.726	9.940	15.029	20.878	26.640
10	18.277	5.912	11.416	14.700	20.808
11	15.941	8.312	12.717	19.873	24.958
12	11.497	6.769	9.538	15.519	18.452
13	34.240	17.556	25.578	37.291	46.551
14	27.551	13.710	20.665	32.043	40.157
15	42.630	22.622	30.780	46.855	57.207
16	35.828	18.766	26.300	42.129	51.878
17	14.422	5.741	9.393	15.072	19.910
18	66.213	32.990	47.399	80.610	101.795
19	33.560	15.081	22.832	35.839	45.541

Table VI

Boundary-Layer Velocity Profile - Configuration 0
(Refer to Table I for Screen Configurations)

Configuration: 0

cm	^y (in.)	U/U _e	cm	^y (in.)	U/U _e
0.159	(0.0625)	0.265	4.572	(1.80)	0.695
0.254	(0.10)	0.292	5.080	(2.00)	0.726
0.381	(0.15)	0.321	5.588	(2.20)	0.755
0.508	(0.20)	0.346	6.096	(2.40)	0.783
0.635	(0.25)	0.366	6.604	(2.60)	0.811
0.762	(0.30)	0.386	7.112	(2.80)	0.836
0.889	(0.35)	0.402	7.620	(3.00)	0.865
1.016	(0.40)	0.418	8.128	(3.20)	0.890
1.143	(0.45)	0.433	8.636	(3.40)	0.912
1.270	(0.50)	0.447	9.144	(3.60)	0.933
1.397	(0.55)	0.460	9.652	(3.80)	0.954
1.524	(0.60)	0.472	10.160	(4.00)	0.970
1.651	(0.65)	0.484	10.668	(4.20)	0.980
1.778	(0.70)	0.496	11.201	(4.410)	0.990
1.905	(0.75)	0.507			
2.032	(0.80)	0.518			
2.159	(0.85)	0.528			
2.286	(0.90)	0.539			
2.413	(0.95)	0.549			
2.540	(1.00)	0.559			
2.794	(1.10)	0.578			
3.048	(1.20)	0.597			
3.302	(1.30)	0.614			
3.556	(1.40)	0.630			
3.810	(1.50)	0.647			
4.064	(1.60)	0.664			
4.318	(1.70)	0.680			

Table VII

Boundary-Layer Velocity Profiles - Configurations 1, 2 and 3
(Refer to Table I for Screen Configurations)

		<u>Configurations:</u>					<u>Configurations:</u>		
	y	1	2	3		y	1	2	3
cm	(in.)	U/U _e	U/U _e	U/U _e	cm	(in.)	U/U _e	U/U _e	U/U _e
0.159	(0.0625)	0.306	0.307	0.317	4.572	(1.8)	0.687	0.682	0.683
0.254	(0.1)	0.323	0.327	0.337	5.080	(2.0)	0.715	0.709	0.707
0.381	(0.15)	0.339	0.351	0.362	5.588	(2.2)	0.740	0.733	0.730
0.508	(0.20)	0.364	0.373	0.383	6.096	(2.4)	0.765	0.756	0.752
0.635	(0.25)	0.383	0.393	0.400	6.604	(2.6)	0.790	0.779	0.771
0.762	(0.30)	0.401	0.412	0.417	7.112	(2.8)	0.814	0.800	0.790
0.889	(0.35)	0.420	0.430	0.433	7.620	(3.0)	0.836	0.820	0.810
1.016	(0.40)	0.436	0.445	0.448	8.128	(3.2)	0.857	0.838	0.827
1.143	(0.45)	0.451	0.459	0.460	8.636	(3.4)	0.877	0.857	0.845
1.270	(0.50)	0.465	0.472	0.473	9.144	(3.6)	0.896	0.875	0.859
1.397	(0.55)	0.477	0.484	0.485	9.652	(3.8)	0.914	0.894	0.874
1.524	(0.60)	0.489	0.495	0.496	10.160	(4.0)	0.930	0.910	0.890
1.651	(0.65)	0.501	0.506	0.507	10.668	(4.2)	0.946	0.924	0.904
1.778	(0.70)	0.512	0.516	0.517	11.176	(4.4)	0.962	0.937	0.917
1.905	(0.75)	0.522	0.525	0.526	11.684	(4.6)	0.975	0.950	0.928
2.032	(0.80)	0.531	0.534	0.535	12.192	(4.8)	0.983	0.963	0.938
2.159	(0.85)	0.540	0.543	0.544	12.652	(4.981)	0.990	-----	-----
2.286	(0.90)	0.550	0.551	0.553	12.700	(5.0)	-----	0.971	0.949
2.413	(0.95)	0.558	0.560	0.561	13.208	(5.2)	-----	0.980	0.960
2.540	(1.00)	0.566	0.567	0.569	13.716	(5.4)	-----	-----	0.970
2.794	(1.1)	0.582	0.583	0.584	13.848	(5.452)	-----	0.990	-----
3.048	(1.2)	0.598	0.599	0.600	14.224	(5.6)	-----	-----	0.978
3.302	(1.3)	0.614	0.613	0.615	14.732	(5.8)	-----	-----	0.985
3.556	(1.4)	0.629	0.627	0.628	15.199	(5.984)	-----	-----	0.990
3.810	(1.5)	0.643	0.641	0.642					
4.064	(1.6)	0.658	0.655	0.656					
4.318	(1.7)	0.672	0.669	0.670					

Table VIII

Boundary-Layer Velocity Profiles - Configurations 4, 5 and 6
(Refer to Table I for Screen Configurations)

y		<u>Configurations:</u>			y		<u>Configurations:</u>		
		4	5	6			4	5	6
cm	(in.)	U/U _e	U/U _e	U/U _e	cm	(in.)	U/U _e	U/U _e	U/U _e
0.159	(0.0625)	0.296	0.300	0.304	4.572	(1.8)	0.678	0.685	0.676
0.254	(0.10)	0.315	0.320	0.327	5.080	(2.0)	0.708	0.712	0.700
0.381	(0.15)	0.336	0.342	0.354	5.588	(2.2)	0.738	0.738	0.725
0.508	(0.20)	0.355	0.362	0.377	6.096	(2.4)	0.765	0.764	0.745
0.635	(0.25)	0.373	0.381	0.396	6.604	(2.6)	0.791	0.787	0.765
0.762	(0.30)	0.391	0.400	0.413	7.112	(2.8)	0.816	0.809	0.786
0.889	(0.35)	0.407	0.418	0.430	7.620	(3.0)	0.840	0.830	0.809
1.016	(0.40)	0.424	0.433	0.446	8.128	(3.2)	0.863	0.850	0.828
1.143	(0.45)	0.440	0.448	0.460	8.636	(3.4)	0.885	0.870	0.847
1.270	(0.50)	0.455	0.461	0.472	9.144	(3.6)	0.905	0.892	0.864
1.397	(0.55)	0.469	0.474	0.484	9.652	(3.8)	0.926	0.910	0.881
1.524	(0.60)	0.481	0.486	0.495	10.160	(4.0)	0.943	0.930	0.897
1.651	(0.65)	0.493	0.498	0.506	10.668	(4.2)	0.958	0.945	0.914
1.778	(0.70)	0.504	0.507	0.516	11.176	(4.4)	0.970	0.961	0.927
1.905	(0.75)	0.514	0.517	0.525	11.684	(4.6)	0.979	0.974	0.940
2.032	(0.80)	0.524	0.527	0.534	12.192	(4.8)	0.988	0.982	0.951
2.159	(0.85)	0.533	0.537	0.543	12.256	(4.825)	0.990	-----	-----
2.286	(0.90)	0.541	0.545	0.550	12.700	(5.0)	-----	-----	0.965
2.413	(0.95)	0.550	0.554	0.558	12.817	(5.046)	-----	0.990	-----
2.540	(1.00)	0.559	0.563	0.565	13.208	(5.2)	-----	-----	0.974
2.794	(1.1)	0.575	0.580	0.580	13.716	(5.4)	-----	-----	0.980
3.048	(1.2)	0.592	0.597	0.595	14.224	(5.6)	-----	-----	0.986
3.302	(1.3)	0.606	0.617	0.609	14.658	(5.771)	-----	-----	0.990
3.556	(1.4)	0.621	0.628	0.624					
3.810	(1.5)	0.635	0.643	0.637					
4.064	(1.6)	0.650	0.657	0.650					
4.318	(1.7)	0.663	0.670	0.664					

Table IX

Boundary-Layer Velocity Profiles - Configurations 7, 8 and 9
(Refer to Table I for Screen Configurations)

		<u>Configurations:</u>					<u>Configurations:</u>		
y		7	8	9	y		7	8	9
cm	(in.)	U/U _e	U/U _e	U/U _e	cm	(in.)	U/U _e	U/U _e	U/U _e
0.159	(0.0625)	0.298	0.296	0.298	5.080	(2.0)	0.703	0.705	0.710
0.254	(0.10)	0.316	0.318	0.320	5.588	(2.2)	0.727	0.732	0.736
0.381	(0.15)	0.336	0.343	0.345	6.096	(2.4)	0.761	0.758	0.761
0.508	(0.20)	0.353	0.361	0.367	6.604	(2.6)	0.791	0.785	0.783
0.635	(0.25)	0.369	0.379	0.386	7.112	(2.8)	0.818	0.811	0.804
0.762	(0.30)	0.385	0.395	0.404	7.620	(3.0)	0.842	0.835	0.826
0.889	(0.35)	0.400	0.411	0.421	8.128	(3.2)	0.868	0.858	0.847
1.016	(0.40)	0.414	0.424	0.436	8.636	(3.4)	0.890	0.880	0.865
1.143	(0.45)	0.427	0.439	0.450	9.144	(3.6)	0.910	0.900	0.881
1.270	(0.50)	0.440	0.452	0.462	9.652	(3.8)	0.928	0.917	0.900
1.397	(0.55)	0.452	0.465	0.474	10.160	(4.0)	0.946	0.933	0.915
1.524	(0.60)	0.464	0.476	0.485	10.668	(4.2)	0.960	0.948	0.931
1.651	(0.65)	0.475	0.488	0.495	11.176	(4.4)	0.975	0.962	0.946
1.778	(0.70)	0.485	0.500	0.505	11.684	(4.6)	0.985	0.974	0.956
1.905	(0.75)	0.496	0.510	0.515	12.118	(4.771)	0.990	-----	-----
2.032	(0.80)	0.506	0.520	0.525	12.192	(4.8)	-----	0.982	0.967
2.159	(0.85)	0.516	0.528	0.534	12.700	(5.0)	-----	-----	0.978
2.286	(0.90)	0.526	0.537	0.543	12.733	(5.013)	-----	0.990	-----
2.413	(0.95)	0.535	0.546	0.552	13.208	(5.2)	-----	-----	0.987
2.540	(1.00)	0.544	0.554	0.560	13.523	(5.324)	-----	-----	0.990
2.790	(1.1)	0.562	0.570	0.576					
3.048	(1.2)	0.579	0.587	0.592					
3.302	(1.3)	0.596	0.603	0.608					
3.556	(1.4)	0.612	0.619	0.624					
3.810	(1.5)	0.628	0.635	0.640					
4.064	(1.6)	0.644	0.650	0.654					
4.318	(1.7)	0.659	0.664	0.670					
4.572	(1.8)	0.674	0.678	0.683					

Table X

Boundary-Layer Velocity Profiles - Configurations 10, 11 and 12
(Refer to Table I for Screen Configurations)

		<u>Configurations:</u>					<u>Configurations:</u>		
y		10	11	12	y		10	11	12
cm	(in.)	U/U _e	U/U _e	U/U _e	cm	(in.)	U/U _e	U/U _e	U/U _e
0.159	(0.0625)	0.309	0.306	0.295	5.080	(2.0)	0.727	0.711	0.703
0.254	(0.10)	0.328	0.326	0.316	5.588	(2.2)	0.753	0.740	0.730
0.381	(0.15)	0.352	0.350	0.341	6.096	(2.4)	0.774	0.766	0.757
0.508	(0.20)	0.372	0.372	0.363	6.604	(2.6)	0.794	0.790	0.786
0.635	(0.25)	0.391	0.390	0.381	7.112	(2.8)	0.816	0.810	0.814
0.762	(0.30)	0.408	0.407	0.400	7.620	(3.0)	0.835	0.830	0.842
0.889	(0.35)	0.424	0.423	0.417	8.128	(3.2)	0.855	0.852	0.863
1.016	(0.40)	0.439	0.436	0.432	8.636	(3.4)	0.874	0.872	0.884
1.143	(0.45)	0.452	0.450	0.446	9.144	(3.6)	0.890	0.890	0.904
1.270	(0.50)	0.465	0.462	0.460	9.652	(3.8)	0.907	0.905	0.920
1.397	(0.55)	0.477	0.474	0.472	10.160	(4.0)	0.922	0.921	0.935
1.524	(0.60)	0.488	0.484	0.483	10.668	(4.2)	0.938	0.935	0.950
1.651	(0.65)	0.499	0.495	0.494	11.176	(4.4)	0.951	0.951	0.964
1.778	(0.70)	0.507	0.504	0.505	11.684	(4.6)	0.964	0.964	0.976
1.905	(0.75)	0.518	0.514	0.515	12.192	(4.8)	0.975	0.975	0.985
2.032	(0.80)	0.528	0.522	0.524	12.489	(4.917)	-----	-----	0.990
2.159	(0.85)	0.538	0.532	0.532	12.700	(5.0)	0.981	0.983	-----
2.286	(0.90)	0.548	0.540	0.541	12.987	(5.113)	-----	0.990	-----
2.413	(0.95)	0.557	0.549	0.550	13.249	(5.216)	0.990	-----	-----
2.540	(1.00)	0.566	0.557	0.558					
2.794	(1.1)	0.585	0.574	0.574					
3.048	(1.2)	0.602	0.590	0.590					
3.302	(1.3)	0.620	0.606	0.605					
3.556	(1.4)	0.637	0.621	0.619					
3.810	(1.5)	0.655	0.636	0.633					
4.064	(1.6)	0.670	0.650	0.647					
4.318	(1.7)	0.685	0.666	0.661					
4.572	(1.8)	0.700	0.682	0.675					

Table XI

Boundary-Layer Velocity Profiles - Configurations 13, 14 and 15
(Refer to Table I for Screen Configurations)

y		<u>Configurations:</u>			y		<u>Configurations:</u>		
		13	14	15			13	14	15
cm	(in.)	U/U _e	U/U _e	U/U _e	cm	(in.)	U/U _e	U/U _e	U/U _e
0.159	(0.0625)	0.314	0.312	0.309	5.080	(2.0)	0.693	0.701	0.685
0.254	(0.10)	0.336	0.332	0.330	5.588	(2.2)	0.716	0.724	0.708
0.381	(0.15)	0.359	0.356	0.353	6.096	(2.4)	0.737	0.748	0.730
0.508	(0.20)	0.380	0.378	0.374	6.604	(2.6)	0.759	0.768	0.751
0.635	(0.25)	0.399	0.397	0.391	7.112	(2.8)	0.780	0.790	0.772
0.762	(0.30)	0.417	0.416	0.409	7.620	(3.0)	0.800	0.810	0.791
0.889	(0.35)	0.433	0.432	0.425	8.128	(3.2)	0.819	0.830	0.811
1.016	(0.40)	0.447	0.446	0.440	8.636	(3.4)	0.837	0.850	0.828
1.143	(0.45)	0.461	0.460	0.453	9.144	(3.6)	0.854	0.867	0.844
1.270	(0.50)	0.473	0.472	0.466	9.652	(3.8)	0.873	0.885	0.862
1.397	(0.55)	0.484	0.484	0.477	10.160	(4.0)	0.889	0.902	0.877
1.524	(0.60)	0.495	0.495	0.488	10.668	(4.2)	0.904	0.917	0.892
1.651	(0.65)	0.505	0.505	0.498	11.176	(4.4)	0.919	0.931	0.907
1.778	(0.70)	0.516	0.514	0.508	11.684	(4.6)	0.933	0.945	0.919
1.905	(0.75)	0.524	0.524	0.517	12.192	(4.8)	0.945	0.957	0.932
2.032	(0.80)	0.532	0.532	0.525	12.700	(5.0)	0.956	0.967	0.944
2.159	(0.85)	0.540	0.540	0.534	13.208	(5.2)	0.966	0.972	0.955
2.286	(0.90)	0.548	0.548	0.541	13.716	(5.4)	0.975	0.985	0.964
2.413	(0.95)	0.556	0.556	0.549	14.224	(5.6)	0.982	0.9895	0.972
2.540	(1.00)	0.564	0.564	0.556	14.288	(5.625)	-----	0.990	-----
2.794	(1.1)	0.578	0.578	0.570	14.732	(5.8)	0.987	-----	0.980
3.048	(1.2)	0.594	0.593	0.585	15.037	(5.920)	0.990	-----	-----
3.302	(1.3)	0.607	0.607	0.599	15.240	(6.0)	-----	-----	0.985
3.556	(1.4)	0.620	0.622	0.612	15.748	(6.2)	-----	-----	0.9895
3.810	(1.5)	0.633	0.635	0.625	15.977	(6.290)	-----	-----	0.990
4.064	(1.6)	0.646	0.648	0.637					
4.318	(1.7)	0.658	0.662	0.650					
4.572	(1.8)	0.671	0.676	0.663					

Table XII

Boundary-Layer Velocity Profiles - Configurations 16, 17 and 18
(Refer to Table I for Screen Configurations)

		Configurations:					Configurations:		
y		16	17	18	y		16	17	18
cm	(in.)	U/U _e	U/U _e	U/U _e	cm	(in.)	U/U _e	U/U _e	U/U _e
0.159	(0.0625)	0.308	0.296	0.309	5.588	(2.2)	0.717	0.754	0.718
0.254	(0.10)	0.328	0.317	0.330	6.096	(2.4)	0.739	0.779	0.735
0.381	(0.15)	0.351	0.340	0.354	6.604	(2.6)	0.761	0.804	0.748
0.508	(0.20)	0.372	0.360	0.376	7.112	(2.8)	0.782	0.825	0.762
0.635	(0.25)	0.391	0.378	0.397	7.620	(3.0)	0.802	0.845	0.777
0.762	(0.30)	0.408	0.395	0.417	8.128	(3.2)	0.821	0.863	0.790
0.889	(0.35)	0.424	0.412	0.436	8.636	(3.4)	0.839	0.878	0.803
1.016	(0.40)	0.438	0.426	0.452	9.144	(3.6)	0.857	0.895	0.816
1.143	(0.45)	0.452	0.439	0.467	9.652	(3.8)	0.873	0.912	0.828
1.270	(0.50)	0.465	0.451	0.477	10.160	(4.0)	0.888	0.929	0.841
1.397	(0.55)	0.476	0.464	0.488	10.668	(4.2)	0.903	0.933	0.853
1.524	(0.60)	0.486	0.475	0.499	11.176	(4.4)	0.916	0.955	0.864
1.651	(0.65)	0.496	0.487	0.508	11.684	(4.6)	0.928	0.969	0.875
1.778	(0.70)	0.506	0.498	0.518	12.192	(4.8)	0.940	0.979	0.888
1.905	(0.75)	0.515	0.509	0.527	12.700	(5.0)	0.952	-----	0.900
2.032	(0.80)	0.523	0.520	0.535	12.817	(5.046)	-----	0.990	-----
2.159	(0.85)	0.532	0.529	0.544	13.208	(5.2)	0.962	-----	0.912
2.286	(0.90)	0.540	0.540	0.552	13.716	(5.4)	0.970	-----	0.923
2.413	(0.95)	0.549	0.550	0.560	14.224	(5.6)	0.978	-----	0.932
2.540	(1.00)	0.556	0.560	0.568	14.732	(5.8)	0.9855	-----	0.941
2.794	(1.1)	0.573	0.577	0.583	15.215	(5.99)	0.990	-----	-----
3.048	(1.2)	0.588	0.597	0.598	15.240	(6.0)	-----	-----	0.950
3.302	(1.3)	0.603	0.614	0.611	15.748	(6.2)	-----	-----	0.956
3.556	(1.4)	0.617	0.631	0.624	16.256	(6.4)	-----	-----	0.964
3.810	(1.5)	0.632	0.649	0.637	16.764	(6.6)	-----	-----	0.973
4.064	(1.6)	0.644	0.665	0.649	17.272	(6.8)	-----	-----	0.980
4.318	(1.7)	0.657	0.681	0.662	17.780	(7.0)	-----	-----	0.984
4.572	(1.8)	0.670	0.696	0.673	18.288	(7.2)	-----	-----	0.988
5.080	(2.0)	0.694	0.725	0.698	18.218	(7.33)	-----	-----	0.990

Table XIII

Boundary-Layer Velocity Profile - Configuration 19
(Refer to Table I for Screen Configurations)

Configuration: 19

y			y		
cm	(in.)	U/U_e	cm	(in.)	U/U_e
0.159	(0.0625)	0.313	5.080	(2.0)	0.699
0.254	(0.10)	0.336	5.588	(2.2)	0.723
0.381	(0.15)	0.356	6.096	(2.4)	0.747
0.508	(0.20)	0.376	6.604	(2.6)	0.770
0.635	(0.25)	0.394	7.112	(2.8)	0.792
0.762	(0.30)	0.411	7.620	(3.0)	0.811
0.889	(0.35)	0.428	8.128	(3.2)	0.831
1.016	(0.40)	0.443	8.636	(3.4)	0.849
1.143	(0.45)	0.457	9.144	(3.6)	0.866
1.270	(0.50)	0.470	9.652	(3.8)	0.882
1.397	(0.55)	0.483	10.160	(4.0)	0.895
1.524	(0.60)	0.494	10.668	(4.2)	0.910
1.651	(0.65)	0.504	11.176	(4.4)	0.924
1.778	(0.70)	0.513	11.684	(4.6)	0.936
1.905	(0.75)	0.523	12.192	(4.8)	0.948
2.032	(0.80)	0.532	12.700	(5.0)	0.958
2.159	(0.85)	0.541	13.208	(5.2)	0.966
2.286	(0.90)	0.550	13.716	(5.4)	0.974
2.413	(0.95)	0.558	14.224	(5.6)	0.982
2.540	(1.00)	0.567	14.732	(5.8)	0.988
2.794	(1.1)	0.582	14.961	(5.89)	0.990
3.048	(1.2)	0.598			
3.302	(1.3)	0.612			
3.556	(1.4)	0.626			
3.810	(1.5)	0.639			
4.064	(1.6)	0.652			
4.318	(1.7)	0.664			
4.572	(1.8)	0.675			

Table XIV
Universal Planar Boundary-Layer Parameters

Configuration No.	$\bar{\Delta}$	$\frac{\bar{\Delta}}{\delta}$	\bar{G}
0	56.91	12.90	19.59
1	58.15	11.67	18.04
2	59.56	10.92	17.08
3	61.52	10.28	16.47
4	59.16	12.26	18.79
5	58.39	11.57	17.95
6	61.35	10.73	16.73
7	60.75	12.73	19.42
8	60.05	11.98	18.48
9	60.67	11.40	17.83
10	57.85	11.09	17.46
11	59.25	11.59	17.82
12	59.66	12.13	18.43
13	64.07	10.82	17.44
14	62.52	11.11	17.78
15	67.67	10.76	17.79
16	65.83	10.99	17.87
17	59.24	11.74	18.30
18	118.91	16.22	9.96
19	63.22	10.73	17.69

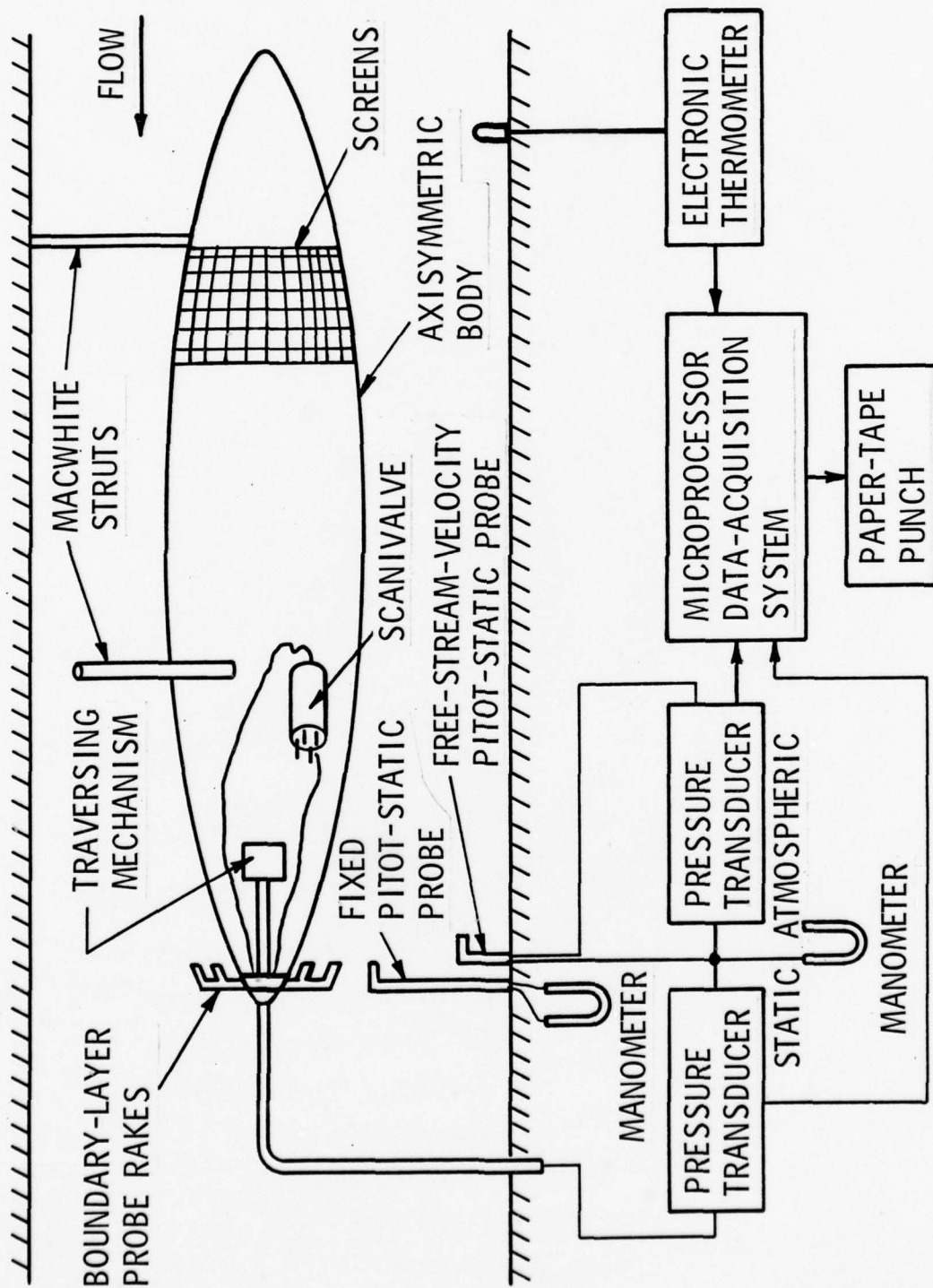


Figure 1 - Schematic of the Axisymmetric Body Mounted in the 1.22-Meter (48-Inch) Diameter Wind Tunnel

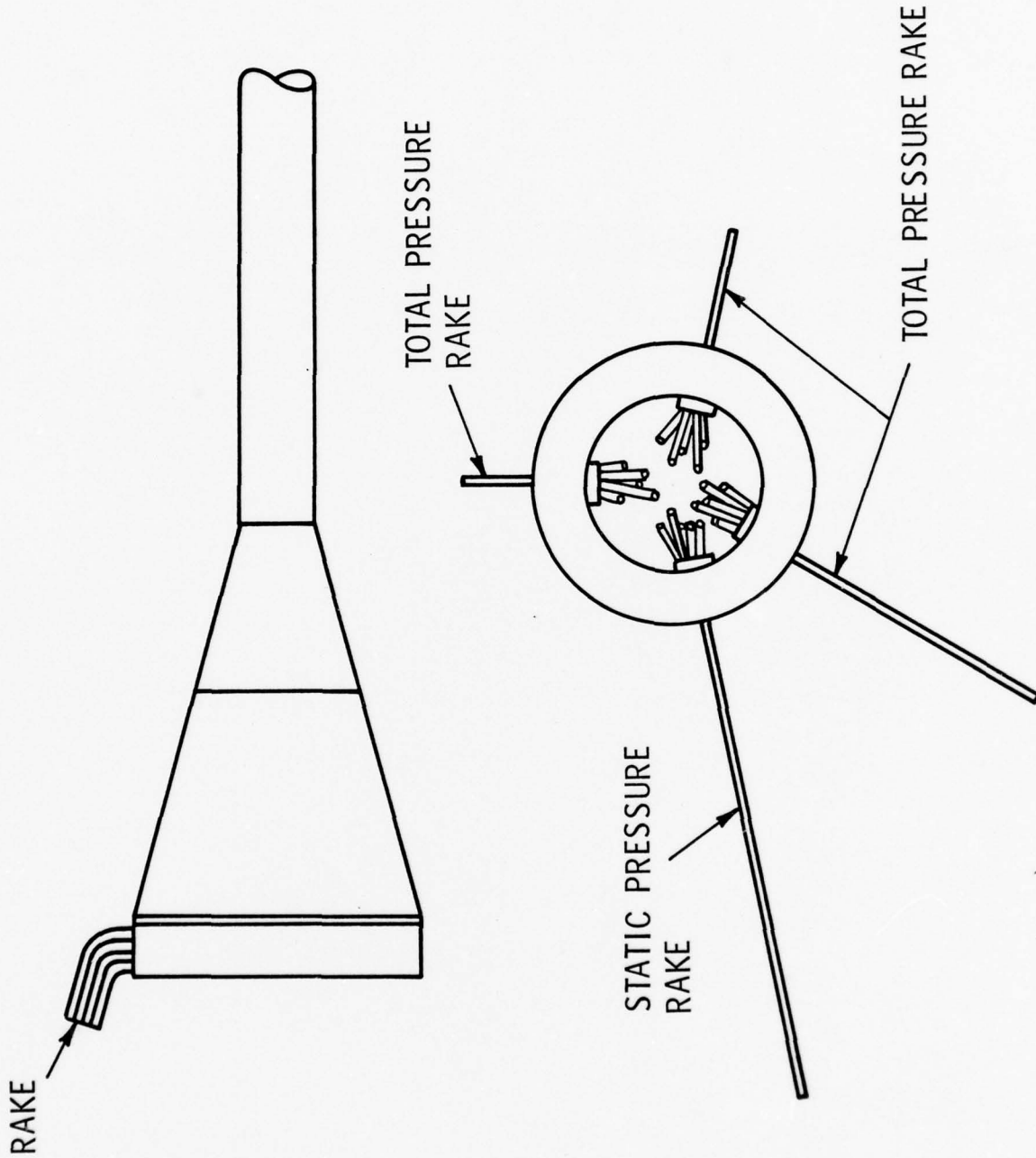


Figure 2 - Schematic of the Probe Rake System

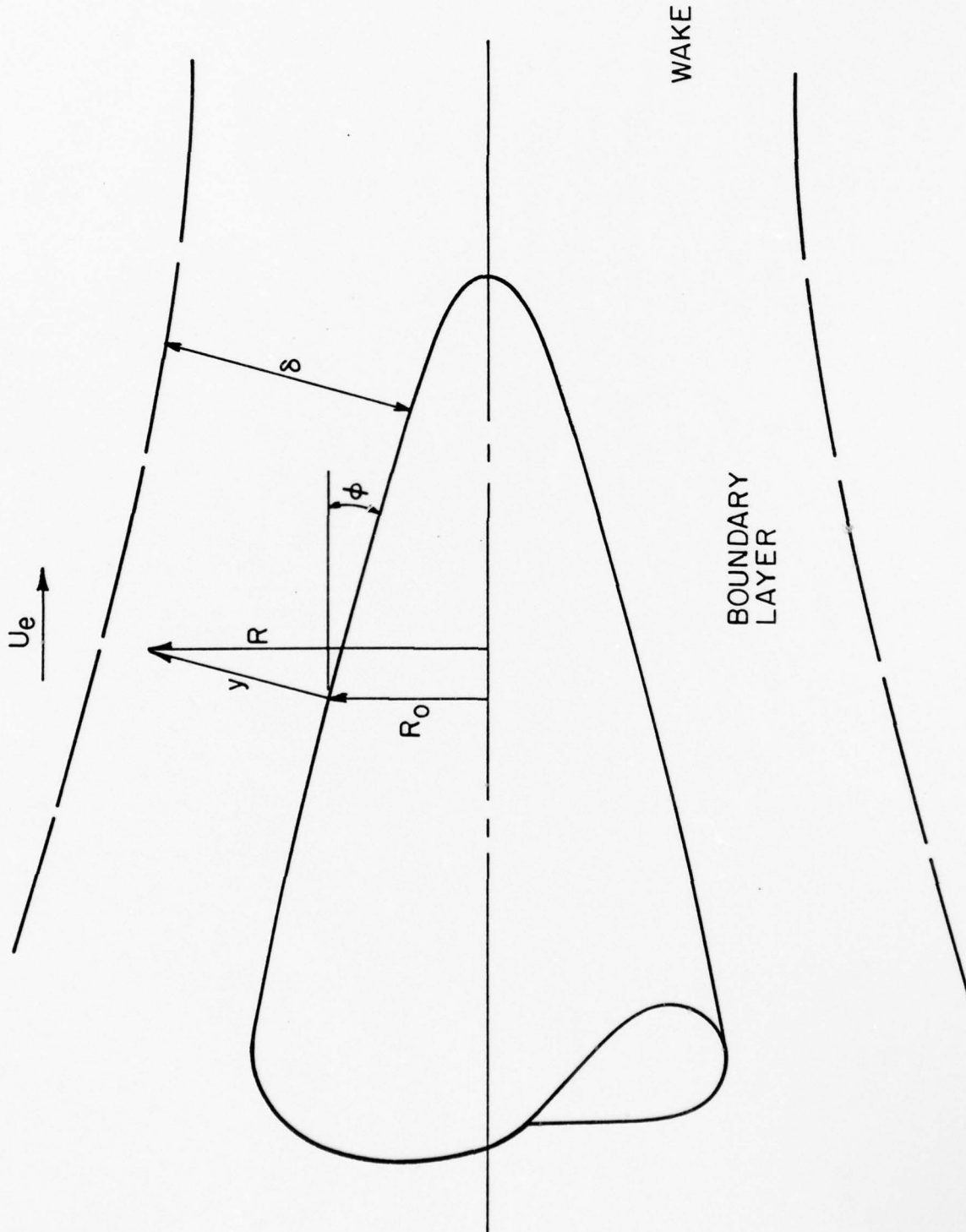


Figure 3 - Thick Axisymmetric Boundary Layer

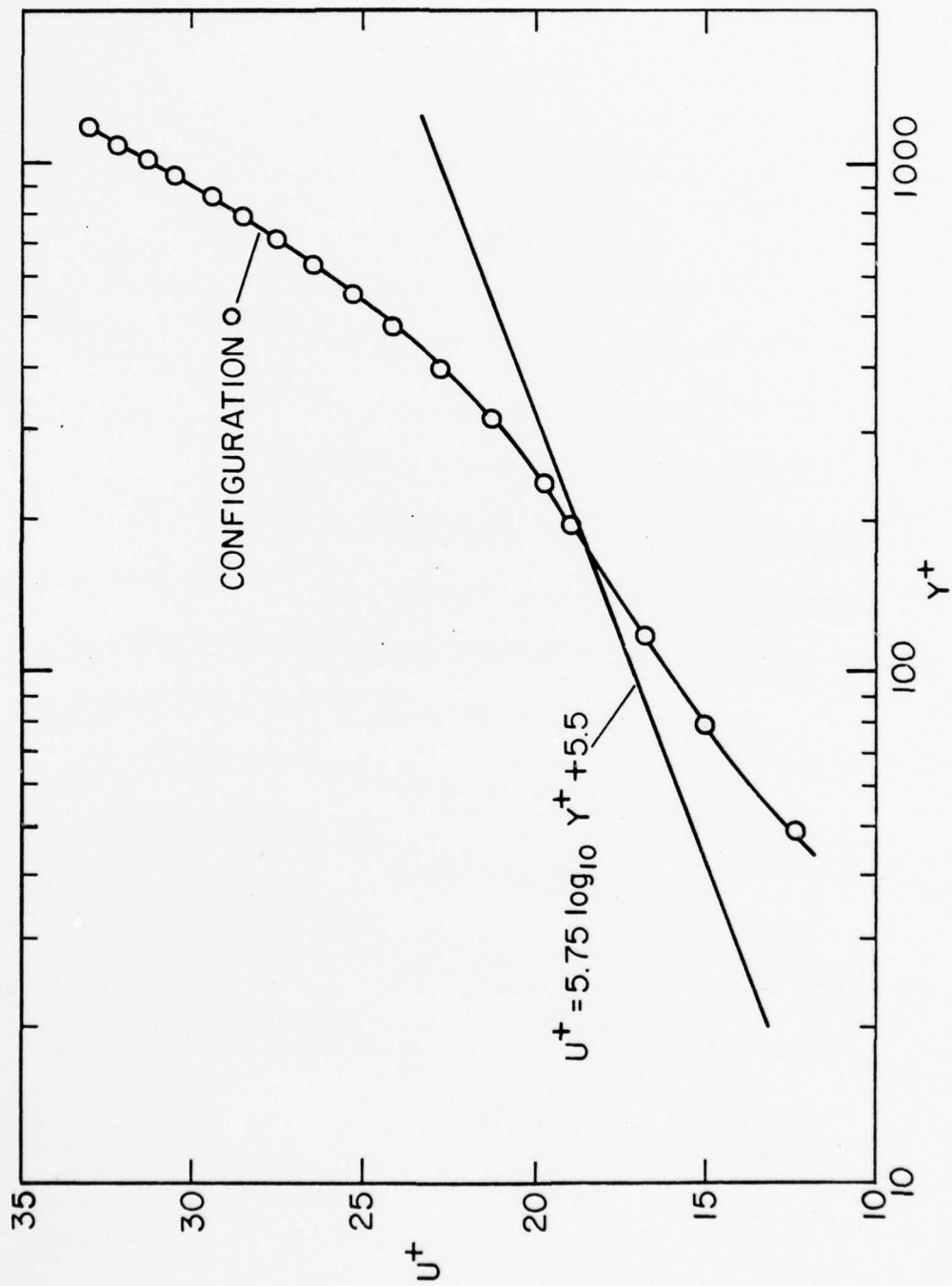


Figure 4 - Law of the Wall for the Bare Body

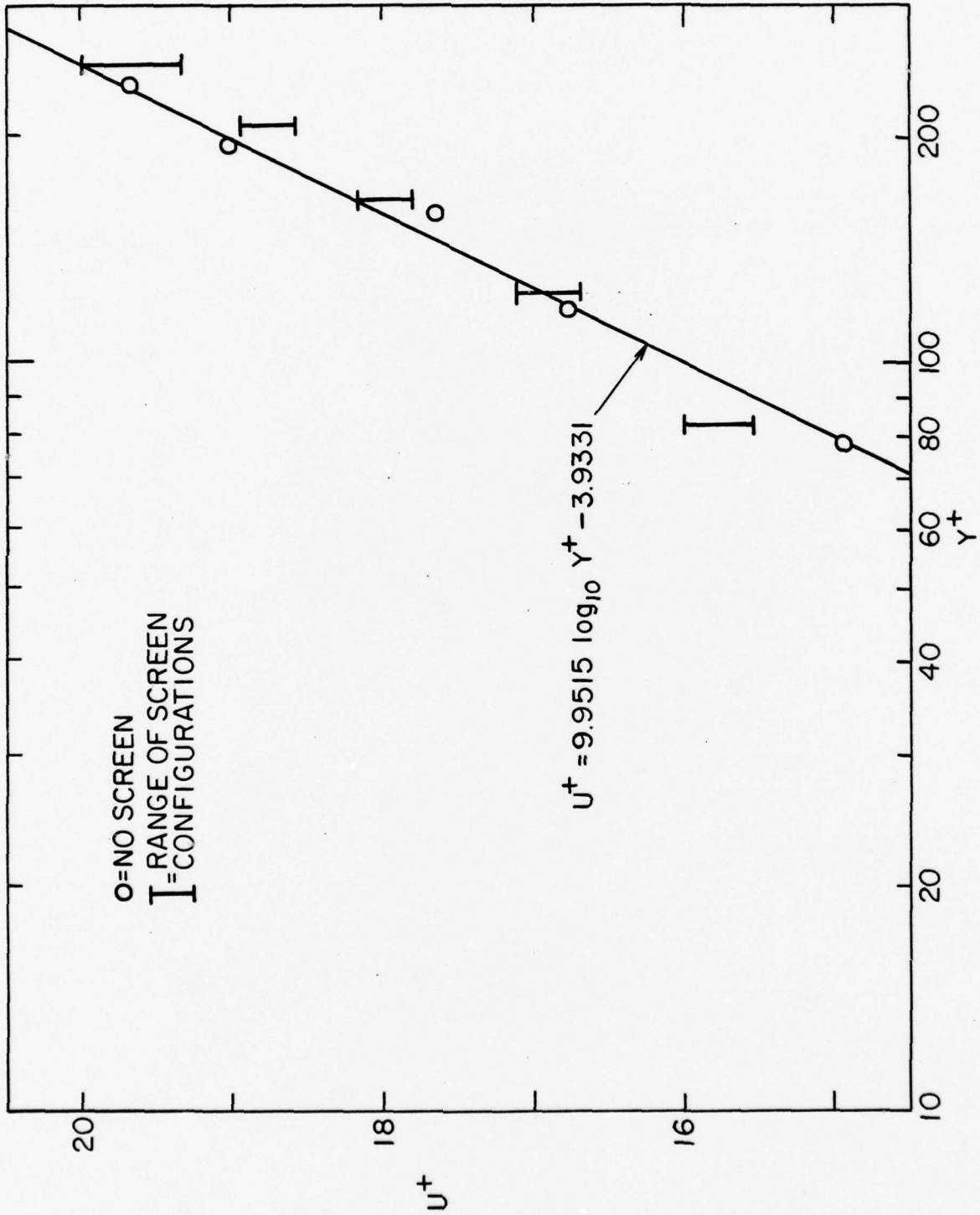


Figure 5 - Screen Data Curve Fit to the Bare Body by the Law of the Wall, Configurations 0 thru 19

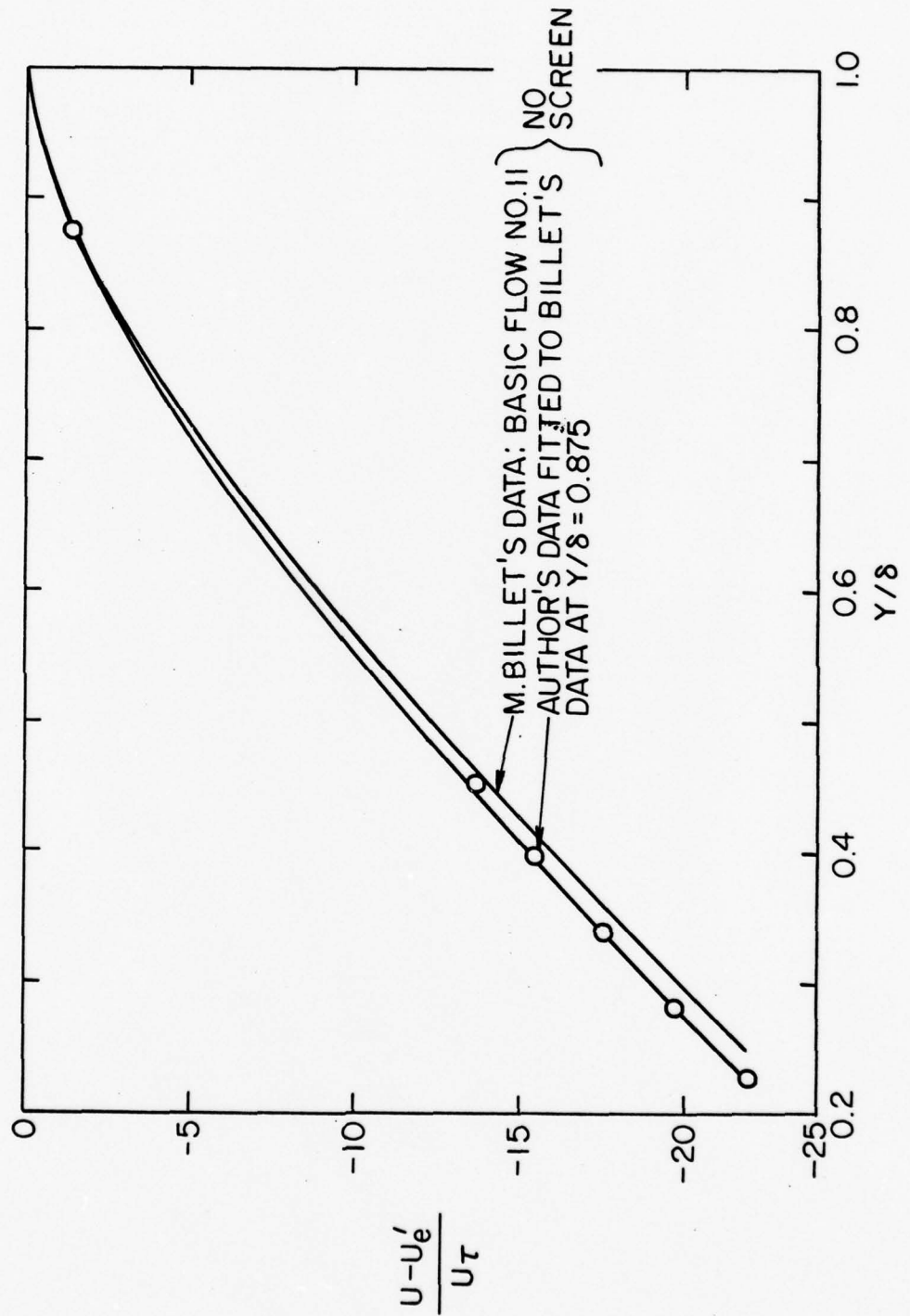


Figure 6 - Velocity Defect Law for the Bare Body

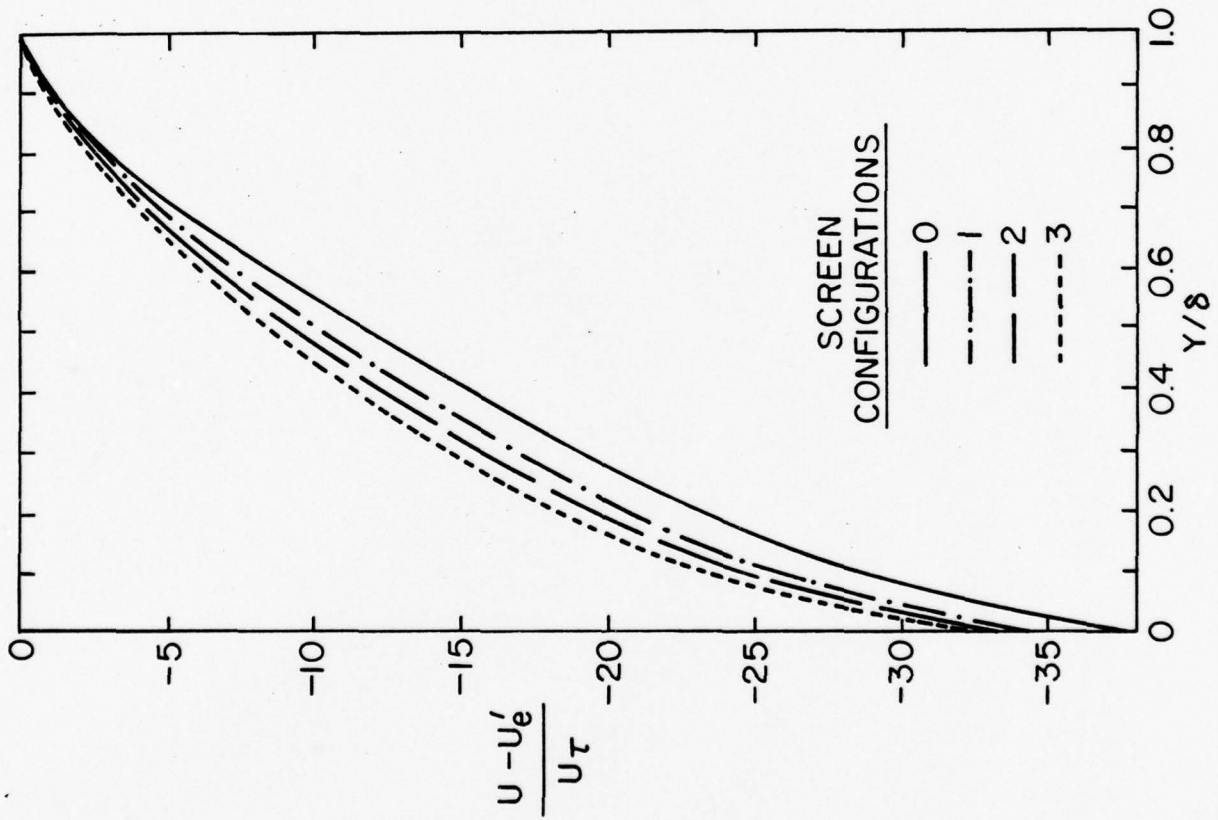


Figure 7 - Velocity Defect Law for Screen Configurations 0, 1, 2, and 3

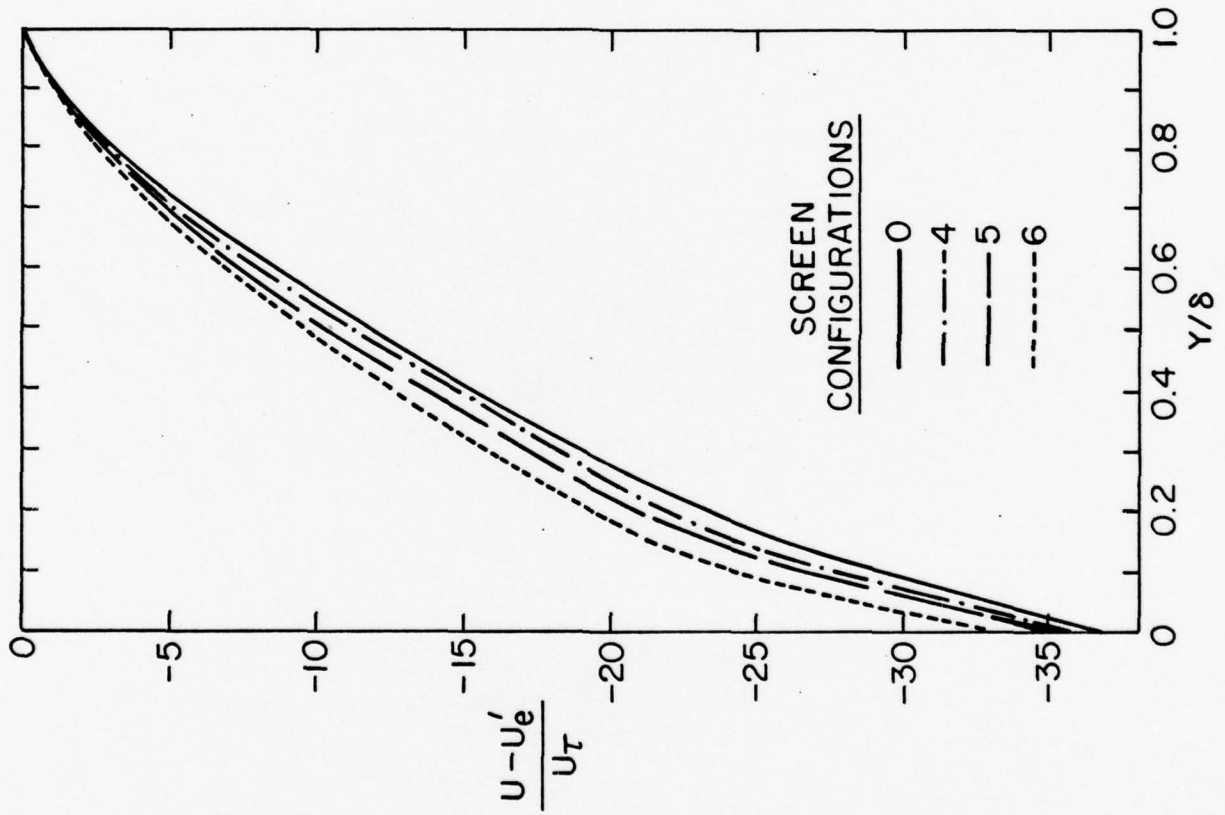


Figure 8 - Velocity Defect Law for Screen Configurations 0, 4, 5, and 6

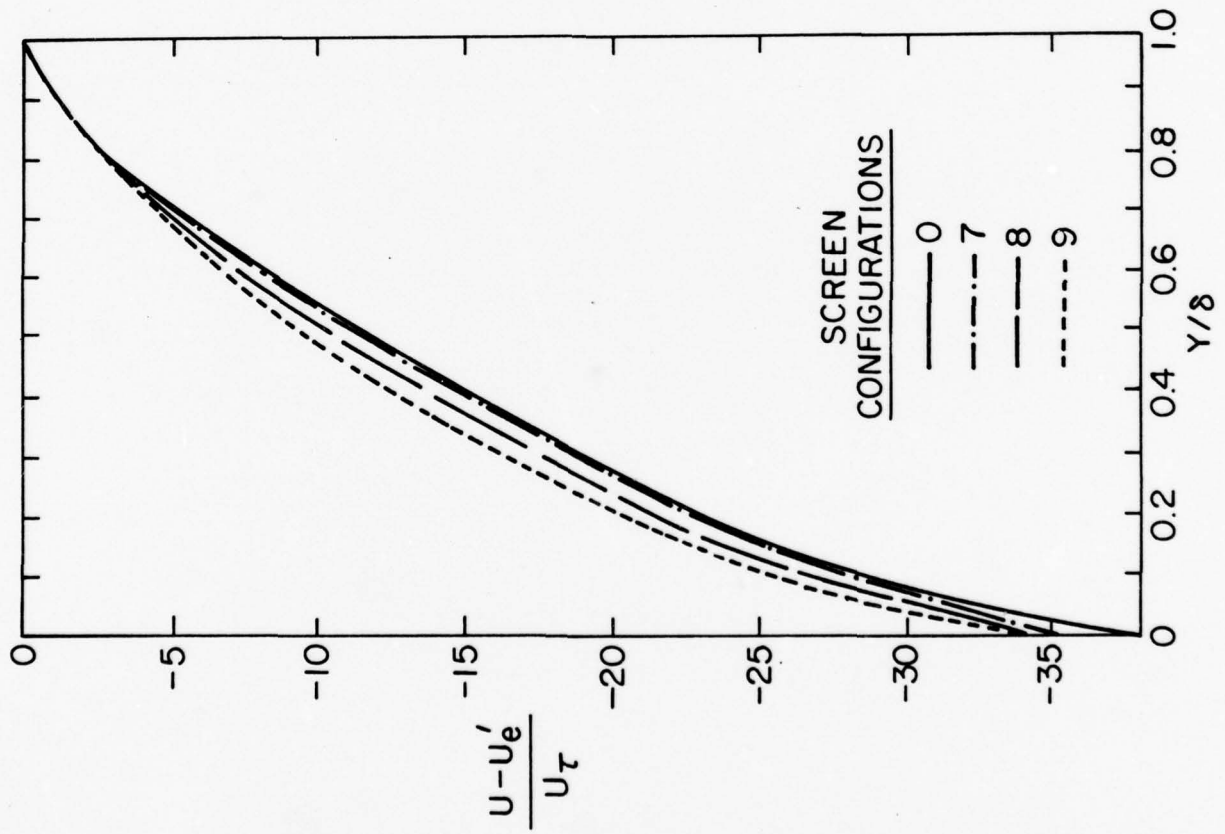


Figure 9 - Velocity Defect Law for Screen Configurations 0, 7, 8, and 9

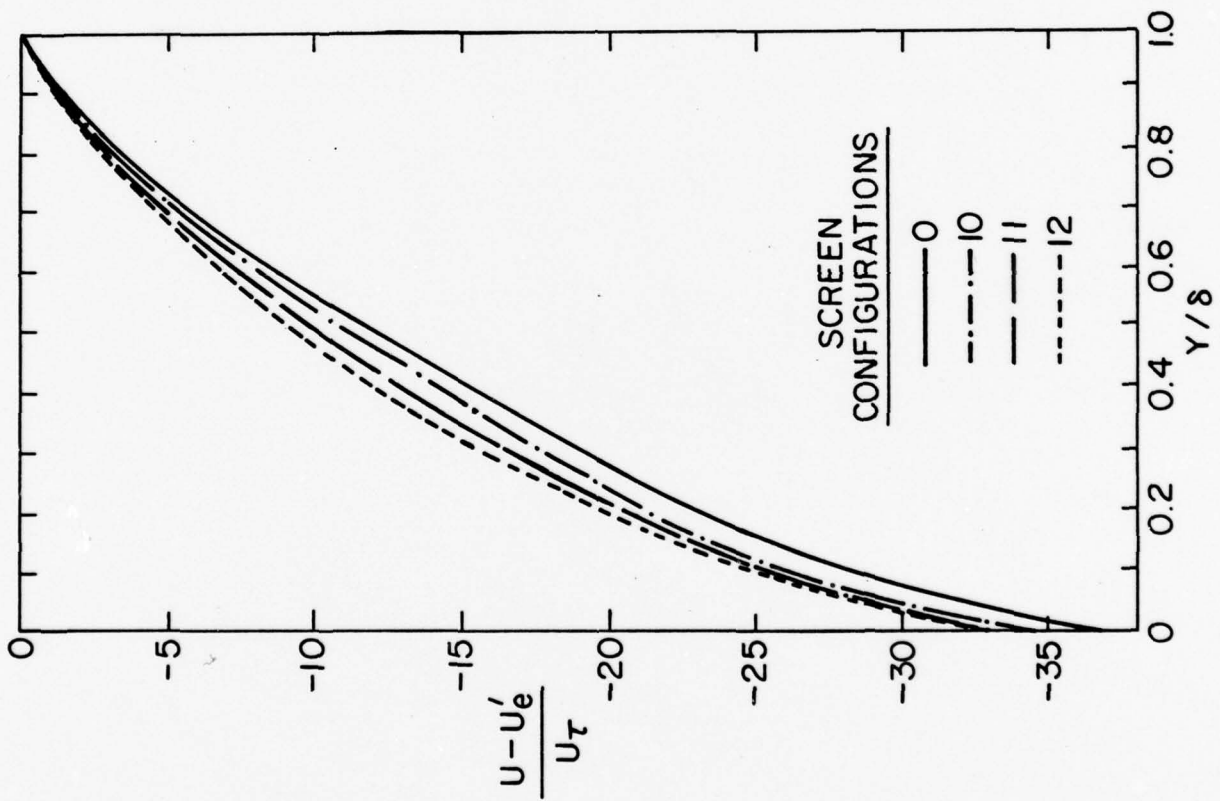


Figure 10 - Velocity Defect Law for Screen Configurations 0, 10, 11, and 12

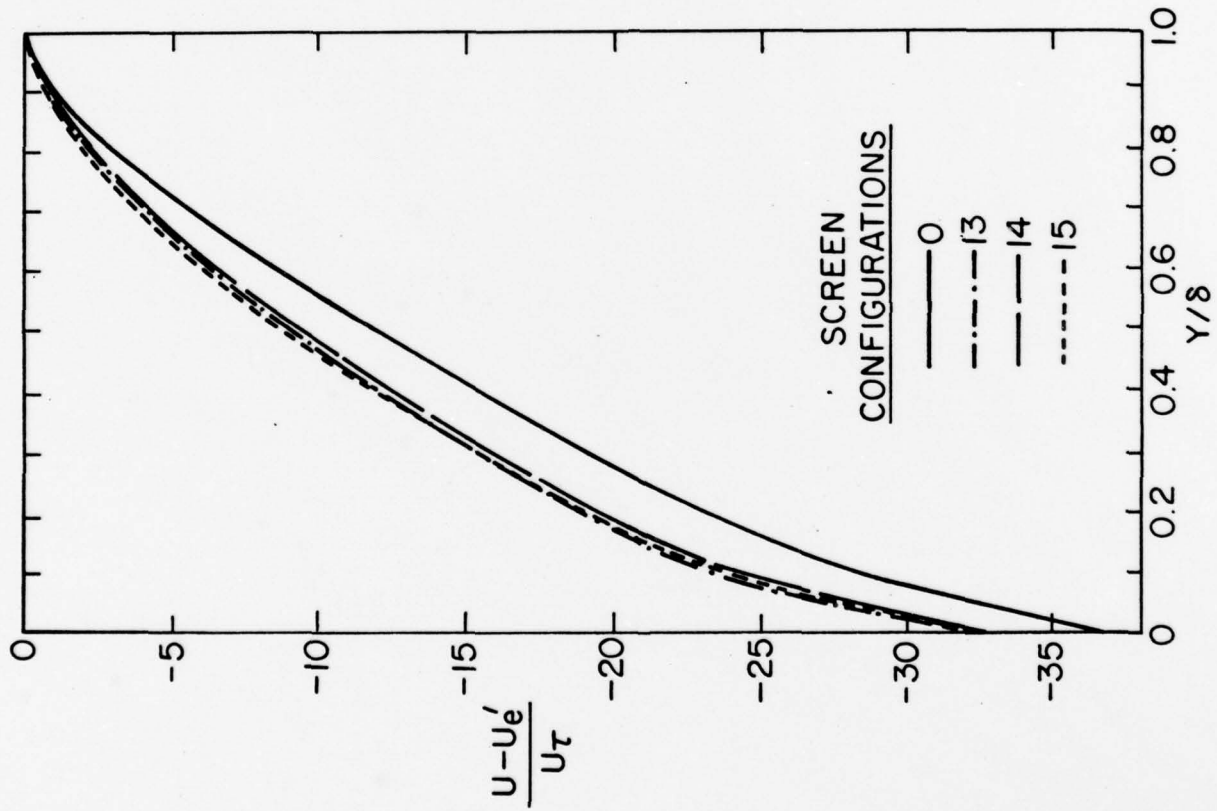


Figure 11 - Velocity Defect Law for Screen Configurations 0, 13, 14, and 15

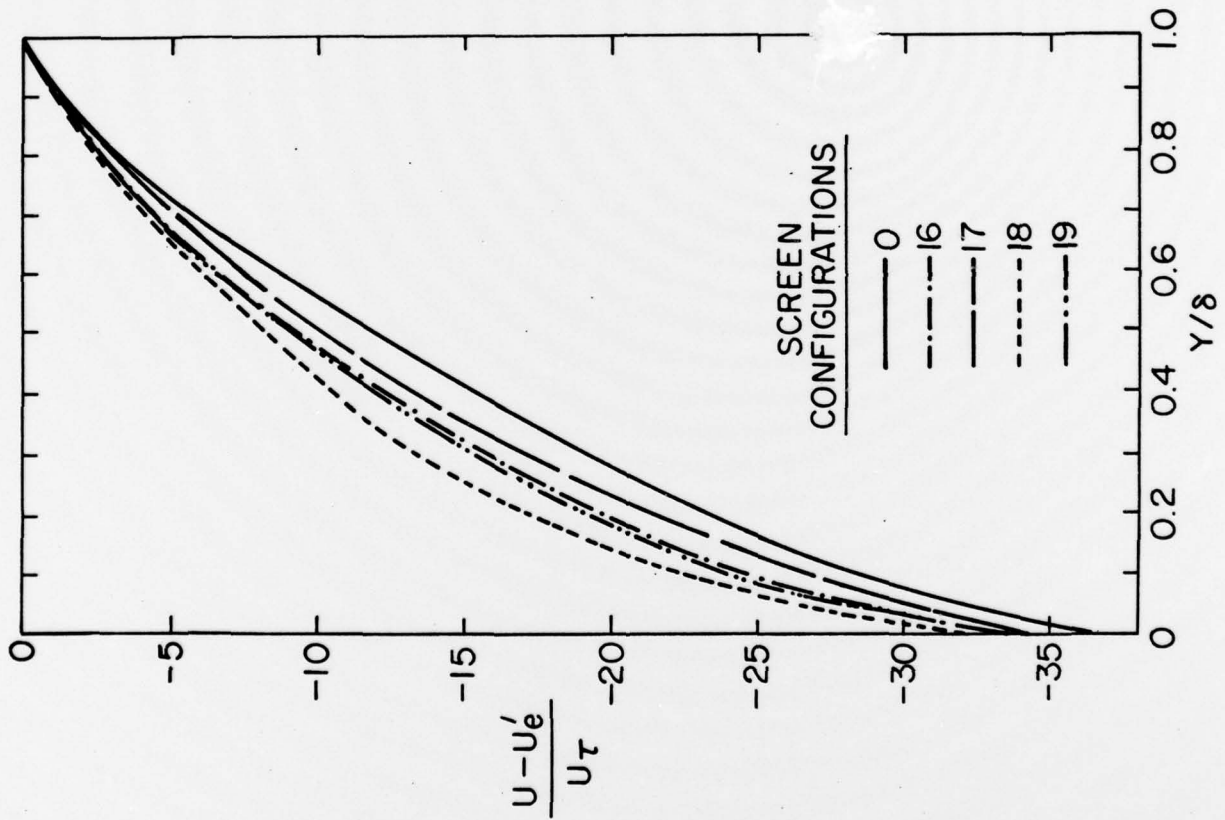


Figure 12 - Velocity Defect Law for Screen Configurations 0, 16, 17, 18, and 19

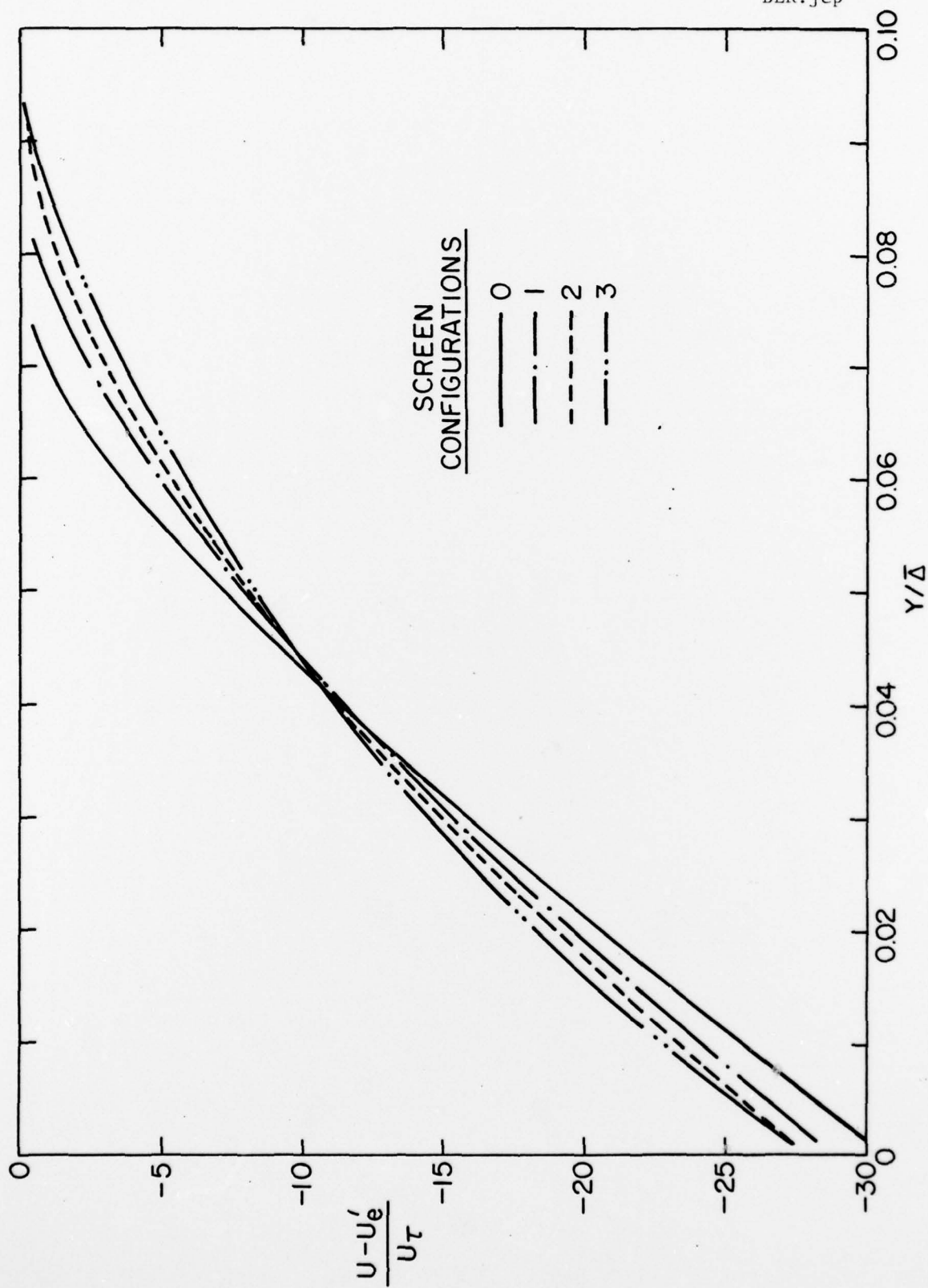


Figure 13 - Equilibrium Velocity Defect Law for Screen Configurations 0, 1, 2, and 3

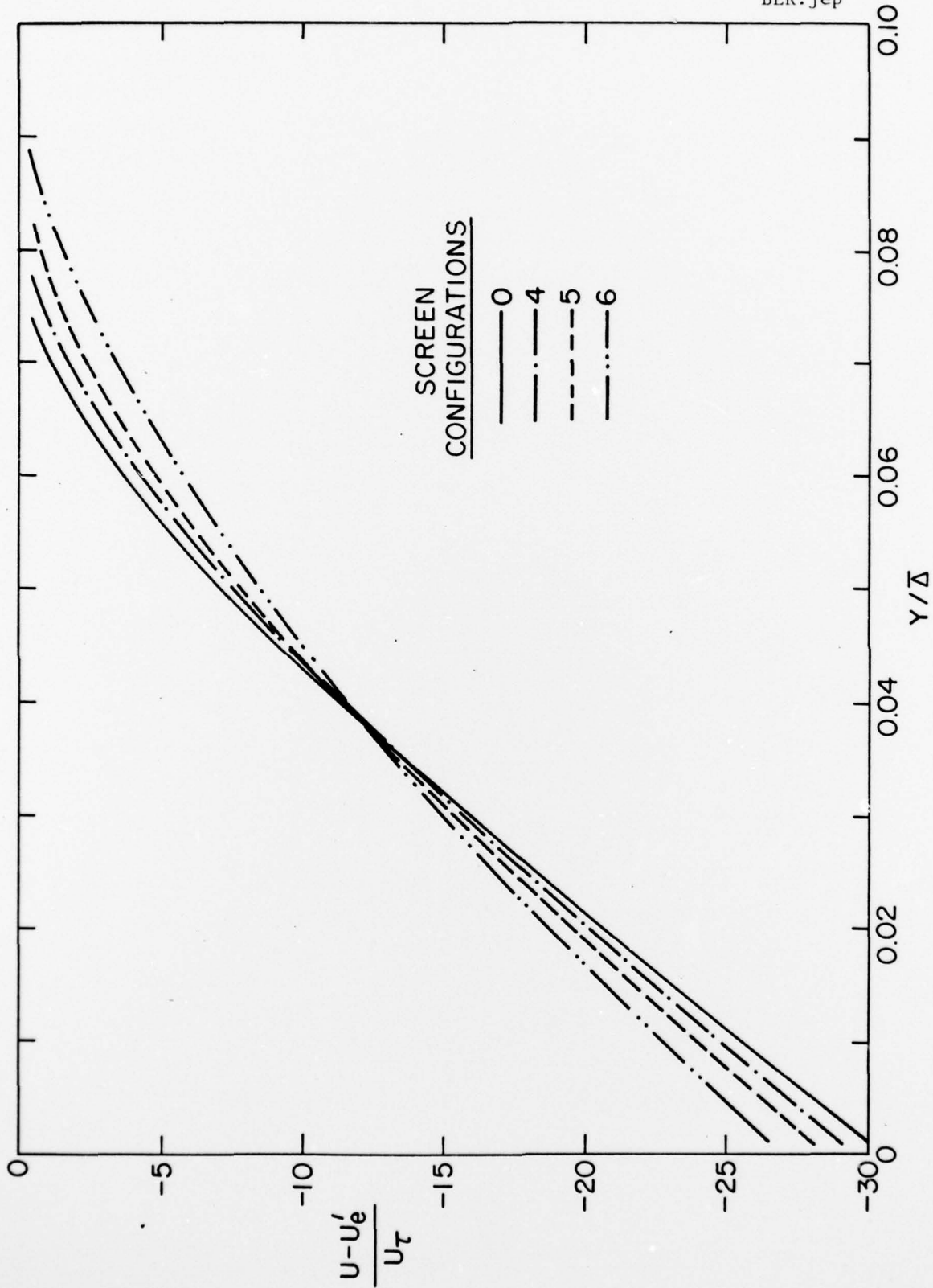


Figure 14 - Equilibrium Velocity Defect Law for Screen Configurations 0, 4, 5, and 6

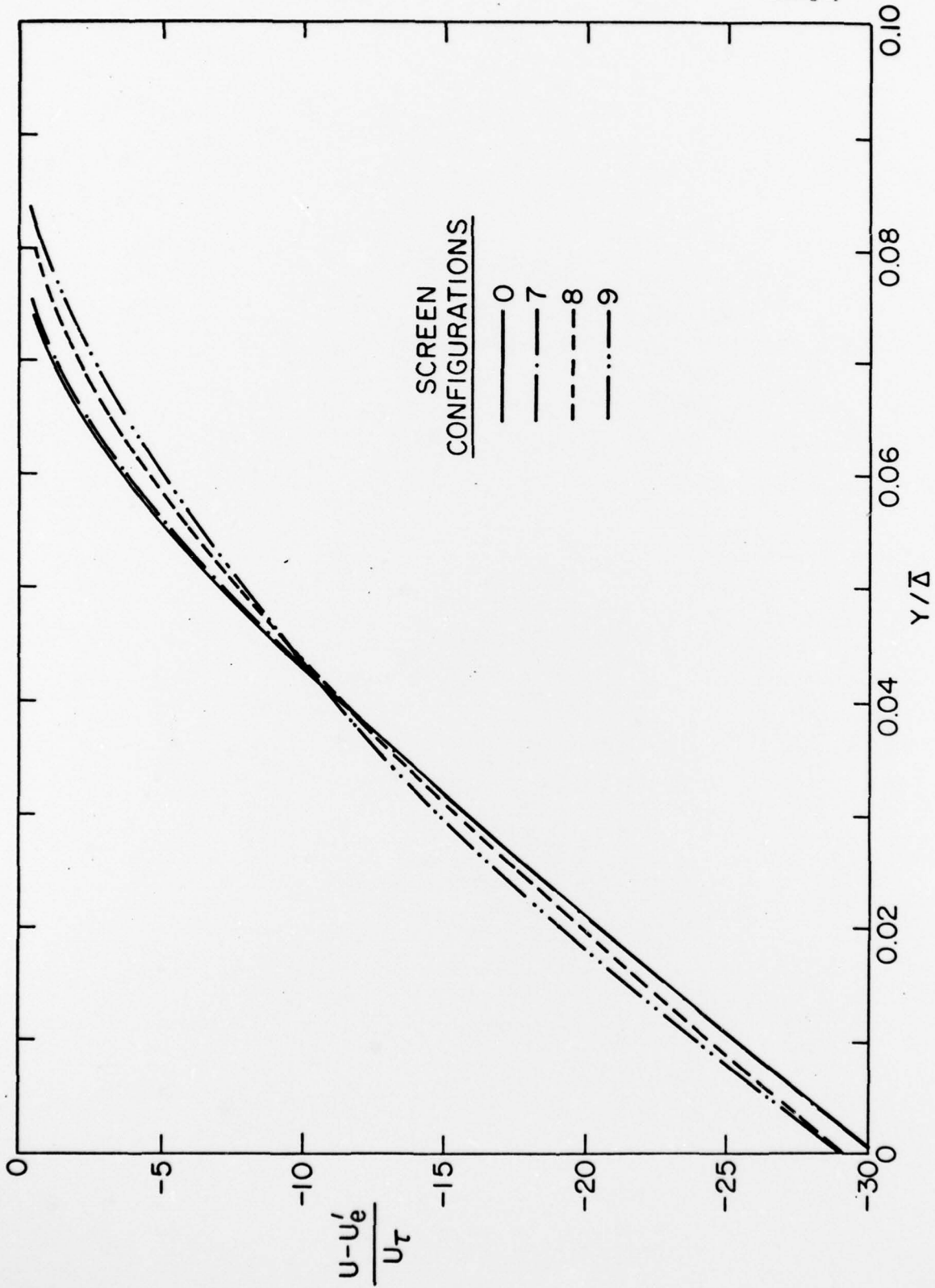


Figure 15 - Equilibrium Velocity Defect Law for Screen Configurations 0, 7, 8, and 9

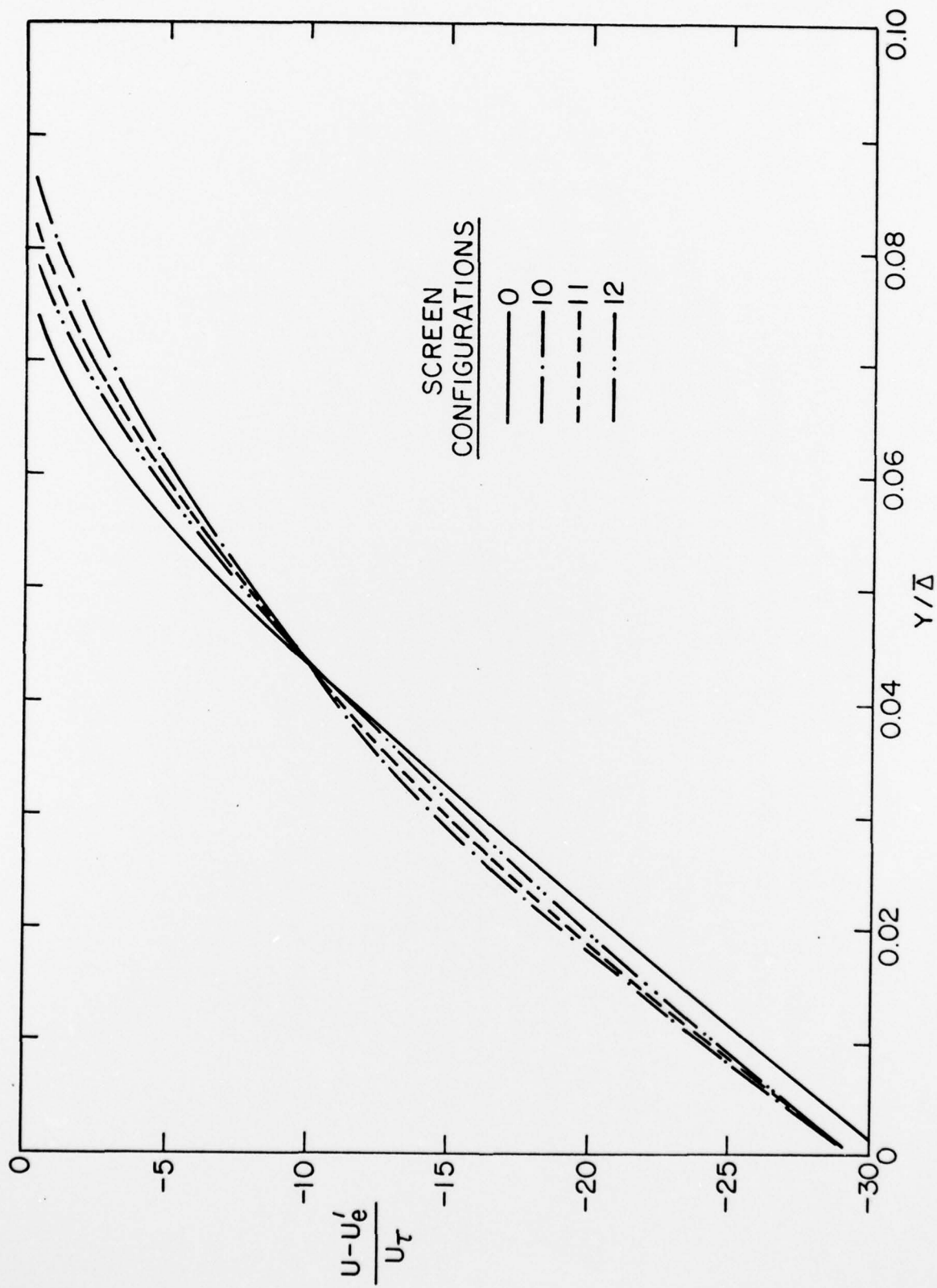


Figure 16 - Equilibrium Velocity Defect Law for Screen Configurations 0, 10, 11, and 12

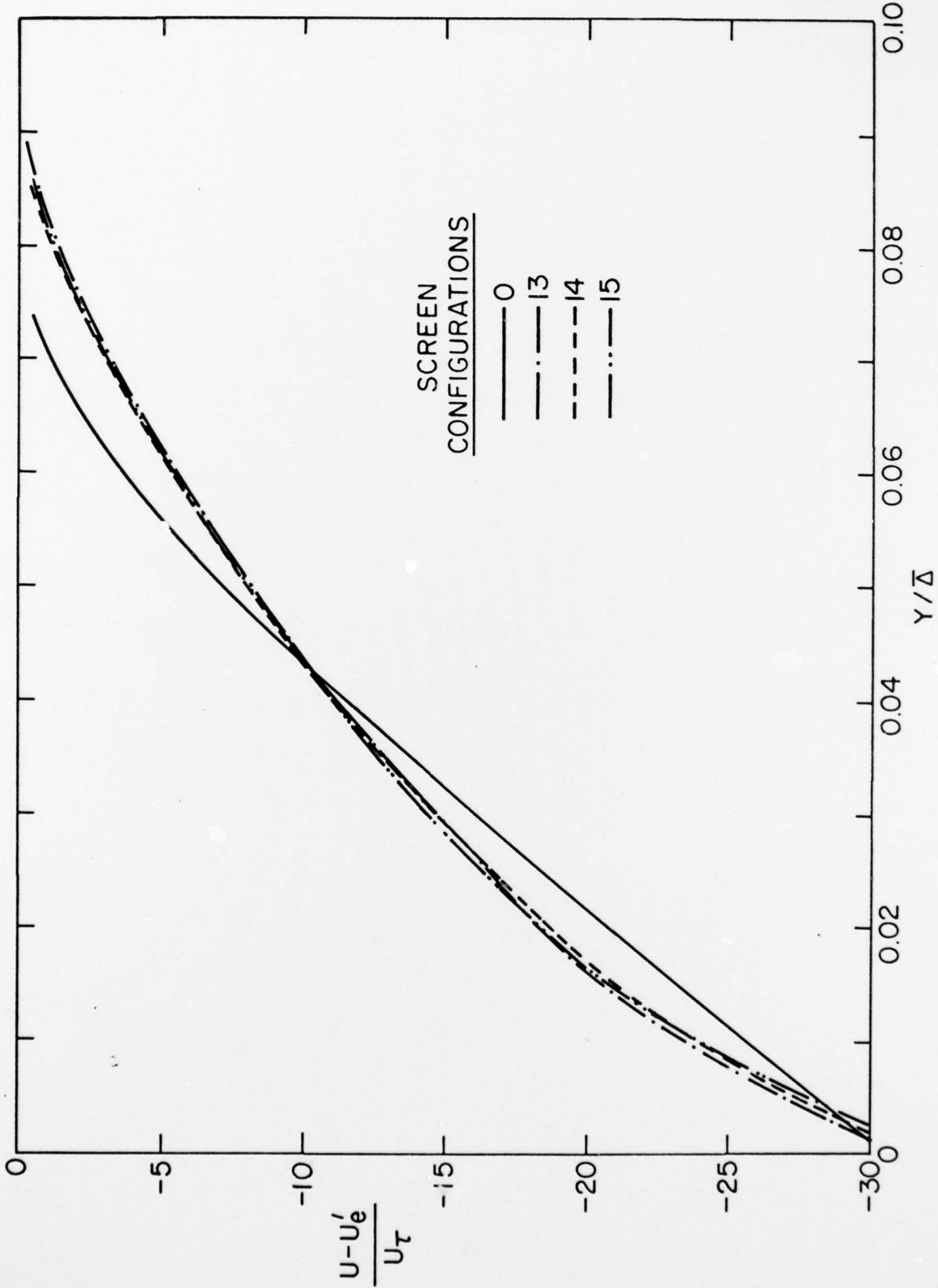


Figure 17 - Equilibrium Velocity Defect Law for Screen Configurations 0, 13, 14, and 15

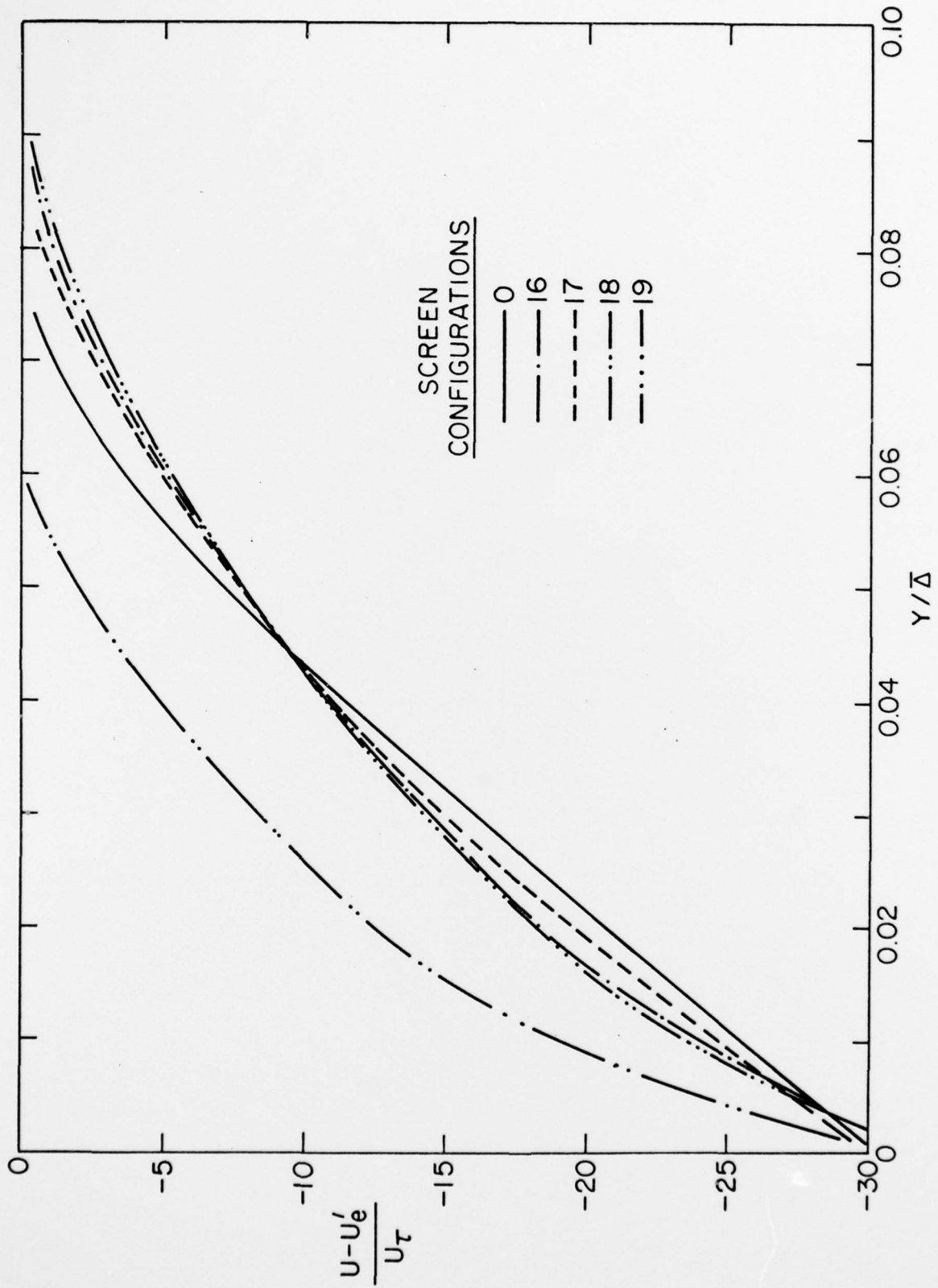


Figure 18 - Equilibrium Velocity Defect Law for Screen Configurations 0, 16, 17, 18, and 19

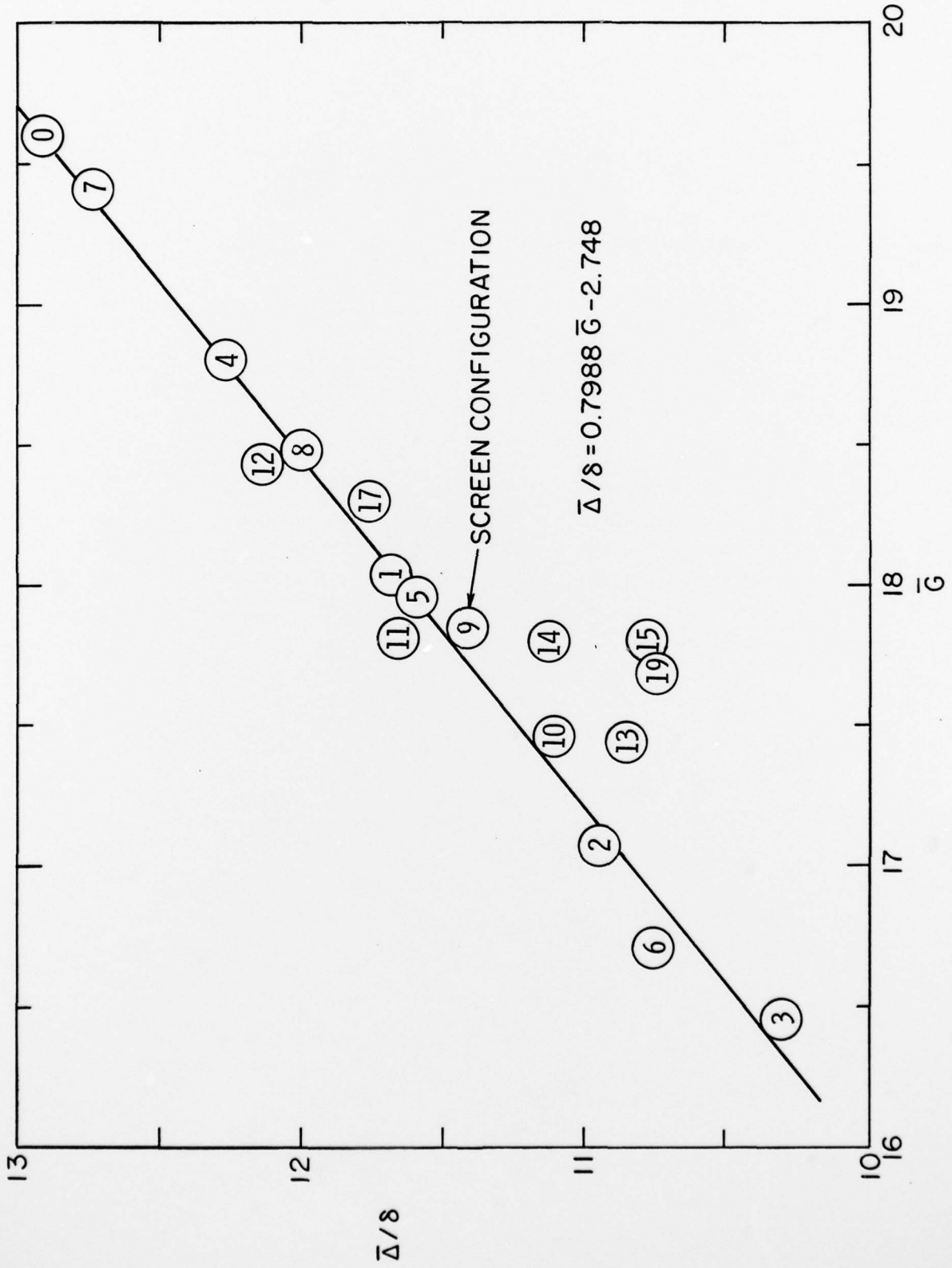


Figure 19 - Universal Plot of $\bar{\Delta}/\delta$ and \bar{G} for All Screen Configurations

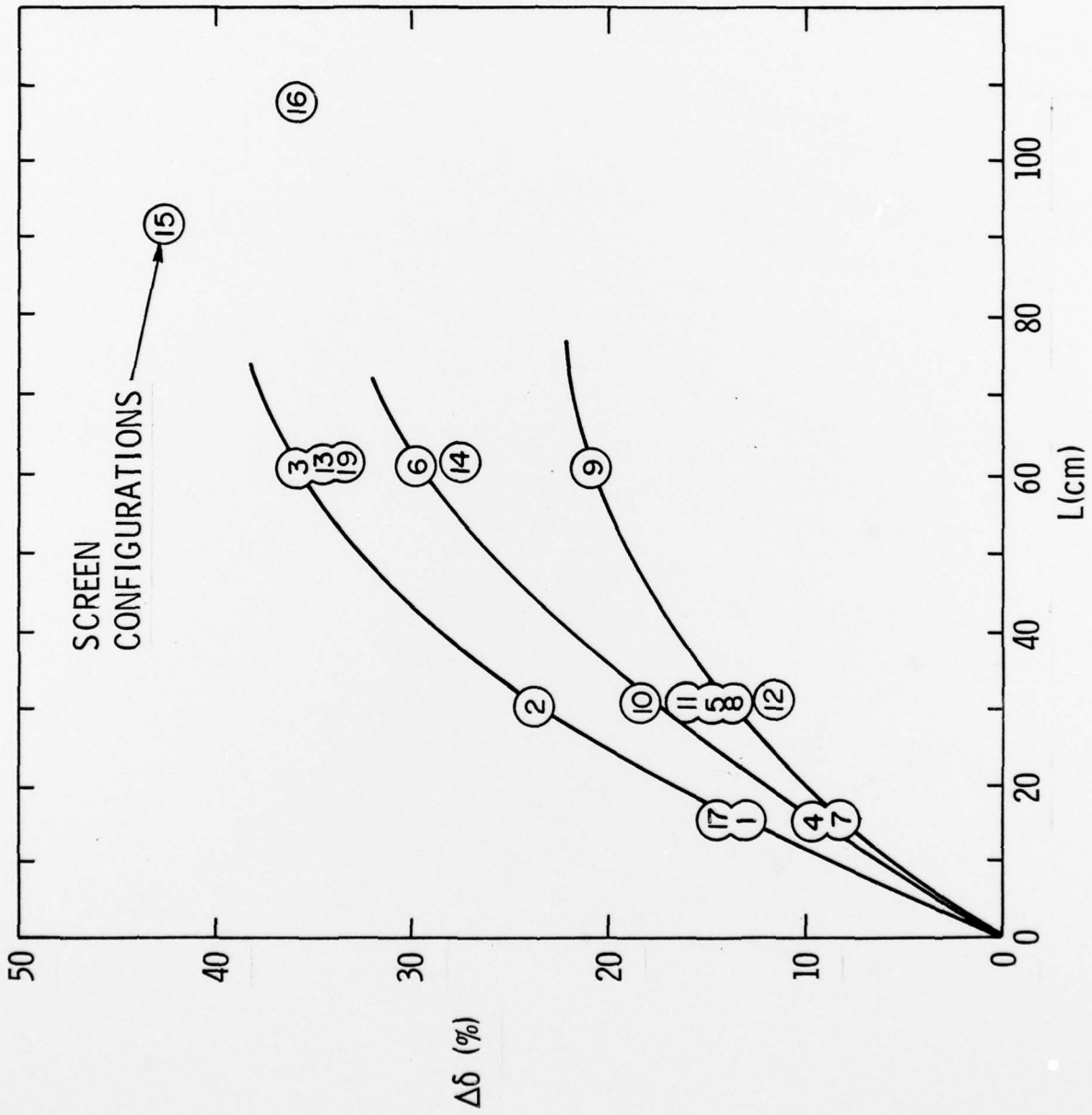


Figure 20 - Effect of Screen Length on Boundary-Layer Thickness Based on the Bare Body

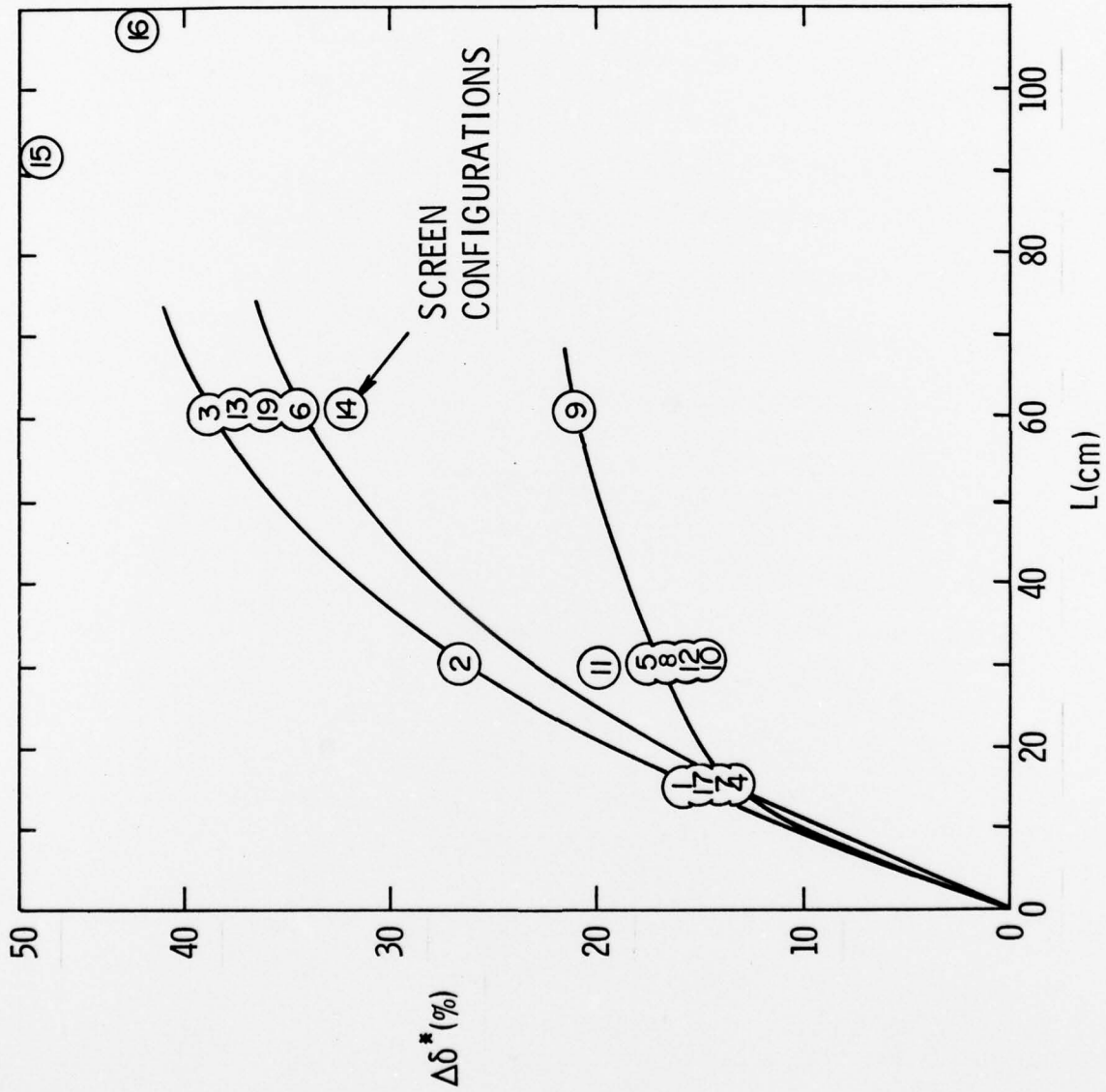


Figure 21 - Effect of Screen Length on the Boundary-Layer Displacement Thickness Based on the Bare Body

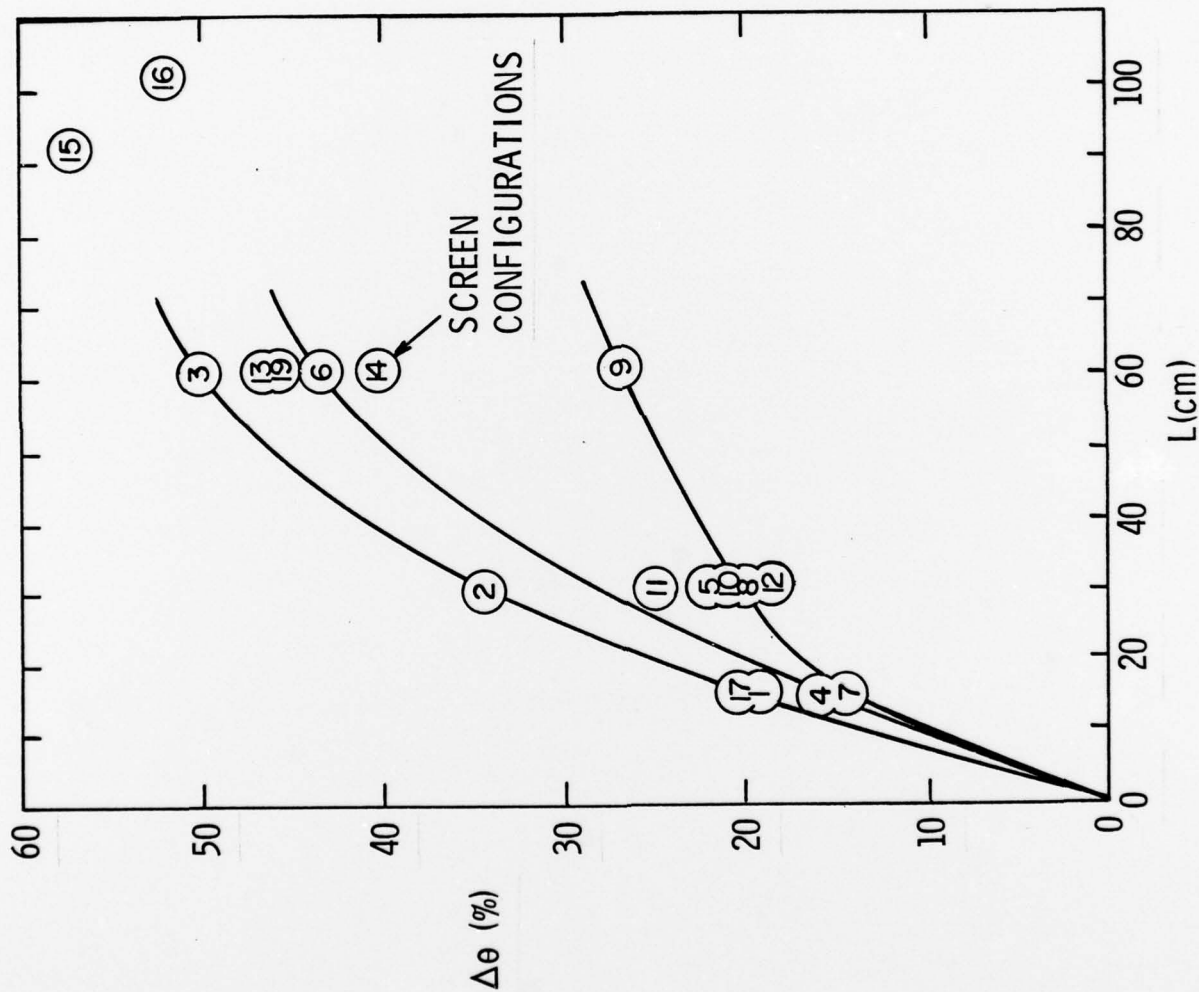


Figure 22 - Effect of Screen Length on the Boundary-Layer Momentum Thickness Based on the Bare Body

DISTRIBUTION LIST FOR UNCLASSIFIED TM 78-64 by B. E. Robbins, dated
24 March 1978

Commander
Naval Sea Systems Command
Department of the Navy
Washington, DC 20362
Attn: Library
Code NSEA-09G32
(Copies No. 1 and 2)

Naval Sea Systems Command
Attn: C. G. McGuigan
Code NSEA-03133
(Copy No. 3)

Naval Sea Systems Command
Attn: T. E. Peirce
Code NSEA-0351
(Copy No. 4)

Naval Sea Systems Command
Attn: J. G. Juergens
Code NSEA-037
(Copy No. 5)

Naval Sea Systems Command
Attn: A. R. Paladino
Code NSEA-0372
(Copy No. 6)

Naval Sea Systems Command
Attn: D. Creed
Code NSEA-03132A
(Copy No. 7)

Commander
Naval Ship Engineering Center
Washington, DC 20362
Attn: W. L. Louis
Code NSEC-6136B
(Copy No. 8)

Naval Ship Engineering Center
Attn: R. J. Cauley
Code NSEC-6140B
(Copy No. 9)

Naval Ship Engineering Center
Attn: F. Welling
Code NSEC-6144
(Copy No. 10)

Naval Ship Engineering Center
Attn: R. M. Petros
Code NSEC-6148
(Copy No. 11)

Naval Ship Engineering Center
Attn: D. Burke
Code NSEC-6140B1
(Copy No. 12)

Commanding Officer
Naval Underwater Systems Center
Newport, RI 02840
Attn: C. N. Pryor
Code 01
(Copy No. 13)

Naval Underwater Systems Center
Attn: D. J. Goodrich
Code 36315
(Copy No. 14)

Naval Underwater Systems Center
Attn: R. N. Nadolink
Code 36315
(Copy No. 15)

Naval Underwater Systems Center
Attn: R. W. Trainor
Code 36314
(Copy No. 16)

Naval Underwater Systems Center
Attn: F. L. White
Code 36301
(Copy No. 17)

Naval Underwater Systems Center
Attn: G. Rossi
Code 36314
(Copy No. 18)

Naval Underwater Systems Center
Attn: Library
Code 54
(Copy No. 19)

DISTRIBUTION LIST FOR UNCLASSIFIED TM 78-64 by B. E. Robbins, dated
24 March 1978

Commanding Officer
Naval Ocean Systems Center
San Diego, CA 92152
Attn: J. W. Hoyt
Code 2501
(Copy No. 20)

Naval Ocean Systems Center
Attn: D. Nelson
Code 2542
(Copy No. 21)

Naval Ocean Systems Center
Attn: A. G. Fabula
Code 5311
(Copy No. 22)

Naval Ocean Systems Center
Attn: M. M. Rieschman
Code 3509
(Copy No. 23)

Commanding Officer and Director
David W. Taylor Naval Ship R&D Center
Department of the Navy
Bethesda, MD 20084
Attn: W. Day
Code 1524
(Copy No. 24)

David W. Taylor Naval Ship R&D Center
Attn: B. Cox
Code 1544
(Copy No. 25)

David W. Taylor Naval Ship R&D Center
Attn: W. E. Cummins
Code 15
(Copy No. 26)

David W. Taylor Naval Ship R&D Center
Attn: R. Wermter
Code 152
(Copy No. 27)

David W. Taylor Naval Ship R&D Center
Attn: W. B. Morgan
(Copy No. 28)

David W. Taylor Naval Ship R&D Center
Attn: R. Cumming
Code 1544
(Copy No. 29)

David W. Taylor Naval Ship R&D Center
Attn: J. McCarthy
Code 1552
(Copy No. 30)

David W. Taylor Naval Ship R&D Center
Attn: Y. T. Shen
Code 1524
(Copy No. 31)

David W. Taylor Naval Ship R&D Center
Attn: M. Sevik
Code 19
(Copy No. 32)

David W. Taylor Naval Ship R&D Center
Attn: W. K. Blake
Code 1942
(Copy No. 33)

David W. Taylor Naval Ship R&D Center
Attn: T. C. Mathews
Code 1942
(Copy No. 34)

David W. Taylor Naval Ship R&D Center
Attn: R. W. Brown
Code 1942
(Copy No. 35)

David W. Taylor Naval Ship R&D Center
Attn: H. T. Wang
Code 1552
(Copy No. 36)

David W. Taylor Naval Ship R&D Center
Attn: E. Caster
Code 1544
(Copy No. 37)

Office of Naval Research
Department of the Navy
800 N. Quincy Street
Arlington, VA 22217
(Copy No. 38)

Defense Documentation Center
5010 Duke Street
Cameron Station
Alexandria, VA 22314
(Copy No. 39 - 50)

DISTRIBUTION LIST FOR UNCLASSIFIED TM 78-64 by B. E. Robbins, dated
24 March 1978

National Bureau of Standards
Aerodynamics Section
Washington, DC 20234
Attn: P. S. Klebanoff
(Copy No. 51)

Rand Corporation
1700 Main Street
Santa Monica, CA 90406
Attn: R. King
(Copy No. 52)

Rand Corporation
Attn: C. Gazley
(Copy No. 53)

Jet Propulsion Laboratory
4800 Oak Grove Drive
Pasadena, CA 91103
Attn: Dr. Leslie M. Mack
(Copy No. 54)

Applied Research Laboratory
The Pennsylvania State University
Post Office Box 30
State College, PA 16801
Attn: M. L. Billet
(Copy No. 55)

Applied Research Laboratory
Attn: R. E. Henderson
(Copy No. 56)

Applied Research Laboratory
Attn: B. E. Robbins
(Copy No. 57)

Applied REsearch Laboratory
Attn: GTWT Library
(Copy No. 58)